Electrochemical Energy Reviews (2024) 7:11
https://doi.org/10.1007/s41918-024-00214-z

REVIEW ARTICLE

Si-Based Anodes: Advances and Challenges in Li-Ion Batteries for Enhanced Stability

Hongshun Zhao[1] · Jianbin Li[1] · Qian Zhao[1] · Xiaobing Huang[2] · Shuyong Jia[1] · Jianmin Ma[3] · Yurong Ren[1]

Received: 21 November 2022 / Revised: 8 October 2023 / Accepted: 31 January 2024

Abstract

Owing to their advantages, such as a high energy density, low operating potential, high abundance, and low cost, rechargeable silicon (Si) anode lithium-ion batteries (LIBs) have attracted considerable interest. Significant advancements in Si-based LIBs have been made over the past decade. Nevertheless, because the cycle instability is a crucial factor in the half/full-battery design and significantly affects the consumption of active components and the weight of the assembled battery, it has become a concern in recent years. This paper presents a thorough analysis of the recent developments in the enhancement methods for the stability of LIBs. Comprehensive in situ and operando characterizations are performed to thoroughly evaluate the electrochemical reactions, structural evolution, and degradation processes. Approaches for enhancing the cycle stability of Si anodes are systematically divided from a design perspective into several categories, such as the structural regulation, interfacial design, binder architecture, and electrolyte additives. The advantages and disadvantages of several methods are emphasized and thoroughly evaluated, offering insightful information for the logical design and advancement of cutting-edge solutions to address the deteriorating low-cycle stability of silicon-based LIBs. Finally, the conclusions and potential future research perspectives for promoting the cycling instability of silicon-based LIBs are presented.

Keywords Lithium-ion batteries · Si-based anodes · Cycling stability · Failure mechanisms · In situ characterization methods · Modification strategies

1 Introduction

Traditional fossil fuels face several challenges, including resource depletion, exploration difficulties, and environmental pollution [1–3]. Multiple efforts have been made toward finding alternative energy sources, and countries such as Germany, France, and England have developed plans to phase out fueled vehicles [4, 5]. Lithium-ion batteries (LIBs) have gained widespread attention owing to their excellent energy density and long lifespan [6–8]. According to the research on energy trends, the worldwide revenue share of electric vehicles is anticipated to increase by 10% by 2025 [9–12]. The current level of LIB industrialization cannot satisfy the rapidly increasing demand for electric and hybrid vehicles; therefore, it is critical to promote ultrahigh energy density LIBs.

Silicon (Si) has attracted considerable interest as an anode because it exhibits excellent characteristics such as abundant resources, environmental friendliness, outstanding reversible capacity, and a relatively suitable operating potential [13–17]. However, Si anodes exhibit large volume changes (> 300%) during lithiation. This large volume expansion causes the bulk Si particles to bear significant tensile stress, which causes surface cracking, fracturing, and pulverization. In addition, it can easily lead to a dynamic electrode-electrolyte interface, further worsening and thickening the solid electrolyte interphase (SEI) [18–20]. Mechanical

✉ Jianmin Ma
nanoelechem@hnu.edu.cn

✉ Yurong Ren
ryrchem@cczu.edu.cn

[1] School of Materials Science and Engineering, Jiangsu Province Engineering Research Center of Intelligent Manufacturing Technology for the New Energy Vehicle Power Battery, Changzhou Key Laboratory of Intelligent Manufacturing and Advanced Technology for Power Battery, Changzhou University, Changzhou 213164, Jiangsu, China

[2] College of Chemistry and Materials Engineering, Hunan University of Arts and Science, Changde 415000, Hunan, China

[3] School of Chemistry, Tiangong University, Tianjin 300387, China

Published online: 10 March 2024

deterioration and SEI instability ultimately result in electrical isolation, poor reversibility, and cyclic capacity decay [21–25]. To date, several approaches have been adopted to address these challenges as much as possible, including the nanomaterial design [26–32], morphology control [33–42], carbon coatings [43–47], and matching suitable battery systems [48–61].

The challenge of cycle instability in LIBs has recently gained growing interest because stability is a key factor in full cell elaboration that significantly affects the availability of active ingredients and the overall mass of the battery after assembly [62–71]. Consequently, the development of Si-based electrodes with enhanced stability has been the focus of recent studies to overcome this constraint and achieve superior electrochemical performance [71–77]. Although considerable attempts have been made to decrease the mechanical strain, few studies have focused on stability [68, 78–81]. Nonetheless, high-quality research has been conducted in relation to the considerable progress of LIBs over recent years; to the best of our knowledge, no special overview has been published that systematically analyzes and categorizes studies that address the problem of the low cycling stability of LIBs. From the perspective of actual implementation, the stability of LIBs is a significant criterion for the energy density when assembling LIBs into complete batteries. Therefore, current research on resolving the stability problem of Si anodes should be extensively analyzed and summarized [82, 83].

This review is the first to comprehensively analyze typical research from the perspective of LIB stability. The failure mechanism during lithiation is analyzed in detail, and the electrochemical reaction process and structural evolution are discussed for various in situ characterization techniques. In addition, we summarize each aspect of the enhanced stability studies with regard to architectural elaboration, interface engineering, innovative binders, and electrolyte additive architectures. Finally, the conclusions and future prospects for the commercialization of Si-based anodes are presented (Fig. 1).

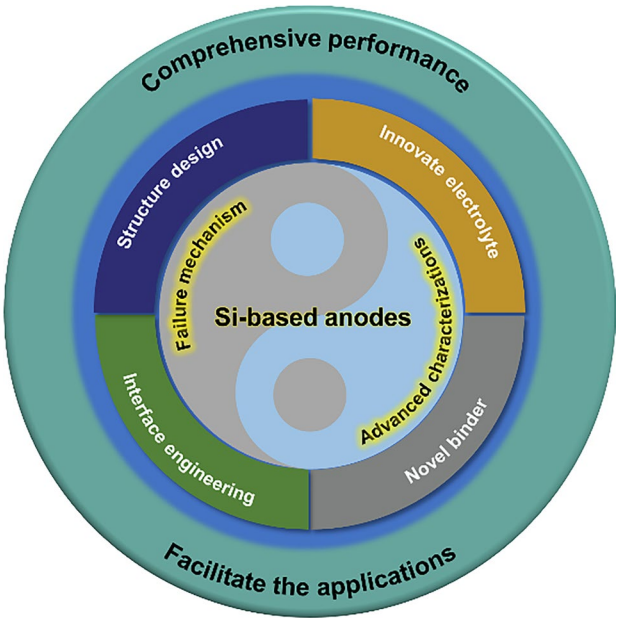

Fig. 1 Scheme of the current advancements in Si-based anode materials

2 Causes of Instability in Si-Based Anodes

Although Si has an extremely high theoretical capacity (Fig. 2a), its cycling properties are quite unstable and it exhibits rapid capacity decay owing to its intrinsic properties (Fig. 2b) [84–86]. Figure 2c depicts the charge-discharge plots of an Si nanoparticle (SiNP) anode at 100 mA g^{-1}. Substantial irreversibility was observed during the initial (de)lithiation process. To analyze the causes of the poor cycling performance, several groups have studied the failure mechanisms of Si anodes [13, 87, 88]. Based on the specific failure process, the failure mechanisms can be divided into mechanical and chemical instabilities.

2.1 Mechanical Instability

Si undergoes a structural transition during initial lithiation, with crystalline Si (c-Si) evolving into amorphous Li_xSi and then into amorphous Si (a-Si) [19, 91–93]. The anisotropic volume changes during lithiation and the shrinkage after delithiation cause the disintegration of Si particles and even disconnect the Si parts from the current collectors or from one another (Figs. 3a and 3b), which is also the main reason for their cycling instability [94–96].

2.2 Chemical Instability

The durability of the SEI at the Si-liquid electrolyte interface is also a major cause of Si anode failure [58, 97–101]. As shown in Fig. 3c, during the first lithiation step, the Si particles shrink, the thin SEI layer dissolves into independent fragments, and the fresh Si anode surface is fully immersed in the electrolyte [102–106]. In the subsequent cycles, a new SEI layer is generated on the freshly uncovered Si surface. A thick SEI layer can increase the electrode impedance/polarization, resulting in a considerably shorter cycle life [107–109].

From this perspective, based on the analysis of the failure mechanism above, we provide the following opinions (Fig. 4). (I) In the first few cycles, the key reason for the rapid capacity decay is the consumption of the Li

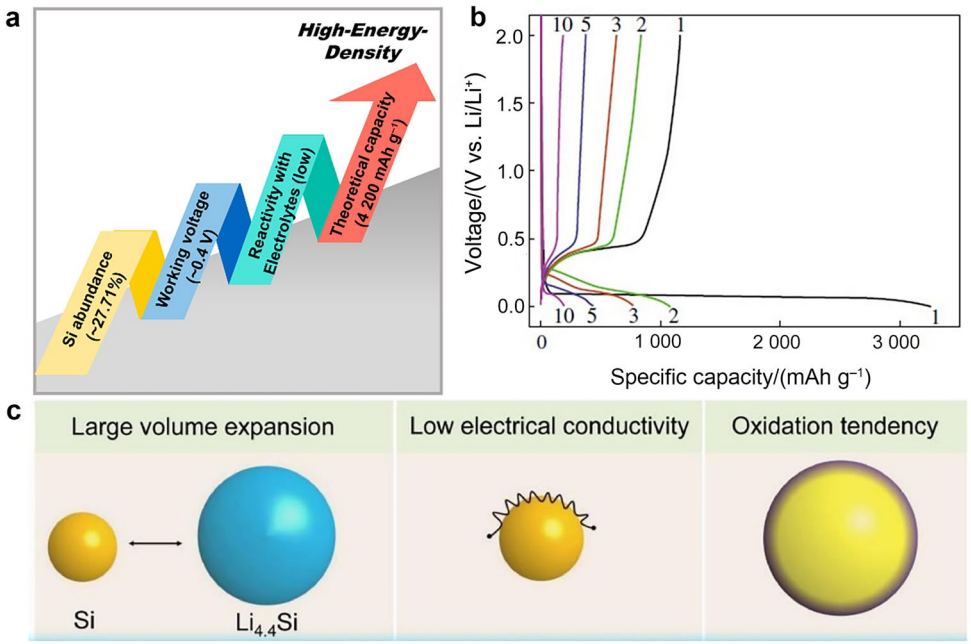

Fig. 2 **a, b** Characteristics of Si-based anodes. Reproduced with permission from Ref. [89]. Copyright © 2004, Elsevier. **c** The initial discharging/charging curve of pristine micro-Si anode materials. Reproduced with permission from Ref. [90]. Copyright © 2022, Elsevier

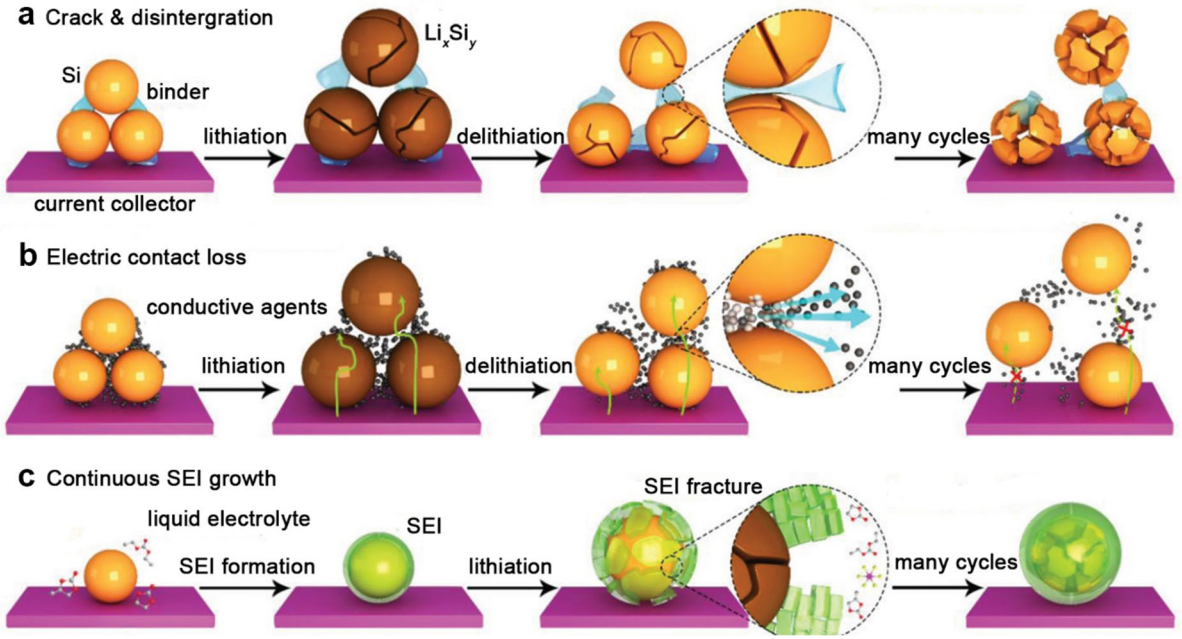

Fig. 3 Primary failure mechanisms of Si-based anodes during (de)lithiation: **a** material pulverization; **b** electrical isolation and thickness swelling; **c** continuous SEI growth. Reproduced with permission from Ref. [110]. Copyright © 2022, Wiley-VCH

inventory. This is primarily due to SEI formation, growth, recombination, and the generation of dead Li. (II) During the subsequent cycling process, the relatively slow decay of the capacity results from the fracture of the Si anodes. (III) The cycling instability in the subsequent long-term cycles is primarily due to the deterioration and flaking of the electrode materials.

3 Advanced In Situ/Operando Characterizations of Silicon-Based Anodes

The failure mechanism of the cycling instability should be thoroughly analyzed by combining various characterization techniques. The two main problems addressed by

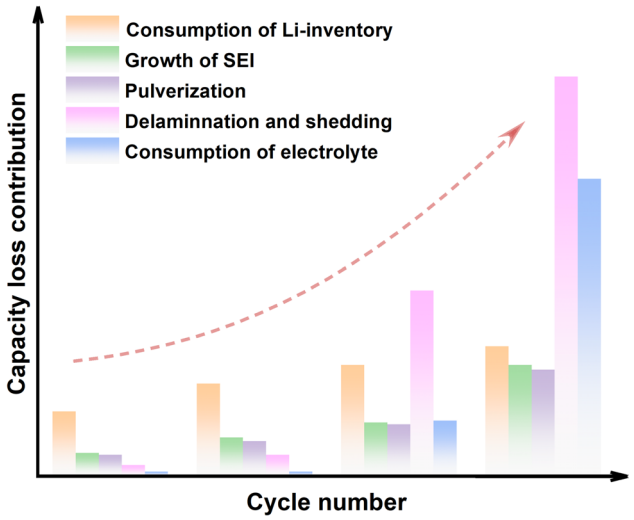

Fig. 4 Scheme of probable failure mechanisms of Si-based anodes during (de)lithiation

advanced characterizations are (1) the evaluation of the morphology and the mechanical performance before and after cycling, and (2) the qualitative or even quantitative analysis of the chemical composition (Fig. 5).

3.1 Characterizations of Morphology and Crystalline Structure

As mentioned in Sect. 2, the instability of the Si anode structure should be thoroughly analyzed during the cycling process. Therefore, the morphological variations, crystal evolution, and Li^+ diffusion modes should be studied. Techniques such as synchrotron X-ray tomography (XRT), X-ray diffraction (XRD), and atomic force microscopy (AFM) can be used to monitor these behaviors. Through these characterizations, researchers can further explain the degradation mechanisms associated with the lithiation process, thereby enhancing the stability of Si anodes.

3.1.1 In Situ Transmission Electron Microscopy

Considering the several microscopic assessment techniques, transmission electron microscopy (TEM) has become a direct and convenient tool for studying the phase and crystal revolution owing to the abundant information on transmission electrons and diffraction. Real-time and atomic-scale changes in SiNPs have been successfully observed by using TEM. The diffusion and phase transformation of Li^+ can also occur during internal Li_xSi alloying. In addition, TEM can be used with component analysis accessories to evaluate the evolution of SEI [74, 111–115].

For Si anodes, mechanical decomposition can be inhibited by using conductive or buffer layers without delaying the Li^+ transmission. From this perspective, the influence of the protective layer on the electrode materials during (de) lithiation can be studied by using in situ TEM to explain the improved cycling stability. He et al. utilized in situ TEM to study the discharging/charging of N-doped carbon coatings on SiNPs (Si@NG spheres) [116]. The in situ TEM revealed that the quasi-isotropic volume expansion varied from 106.98 to 125.58 nm during the initial lithiation (Figs. 6a–6c). In addition, a 2–3-nm SEI layer was generated, which was stable after 200 s of lithiation (Figs. 6d–6f). In addition, the morphological changes in the NG layer were observed in real time. As shown in Figs. 5g–5i, when a tungsten wire was pressed close to the NG shell, it was compressed along the

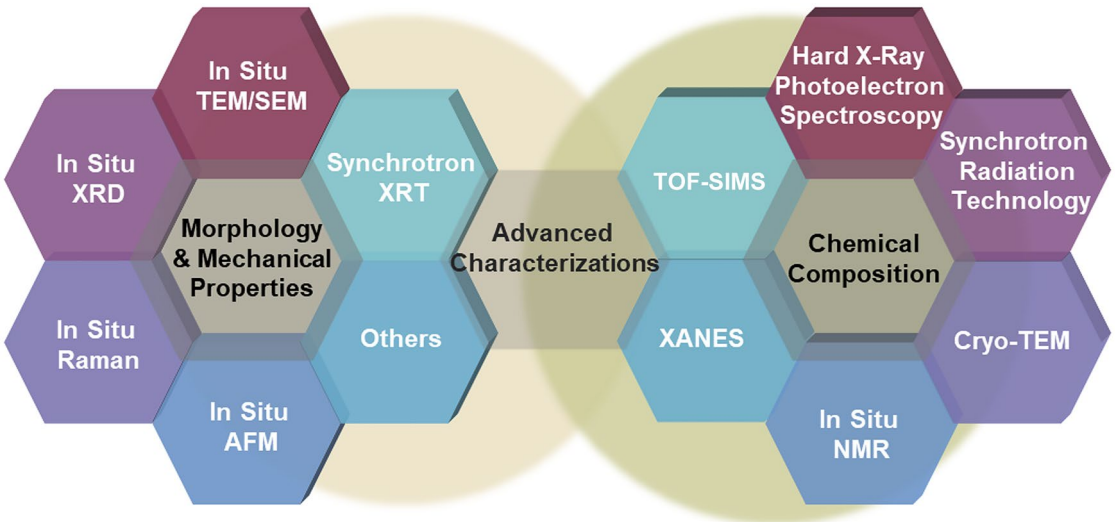

Fig. 5 Advanced in situ/operando characterizations of failure mechanisms

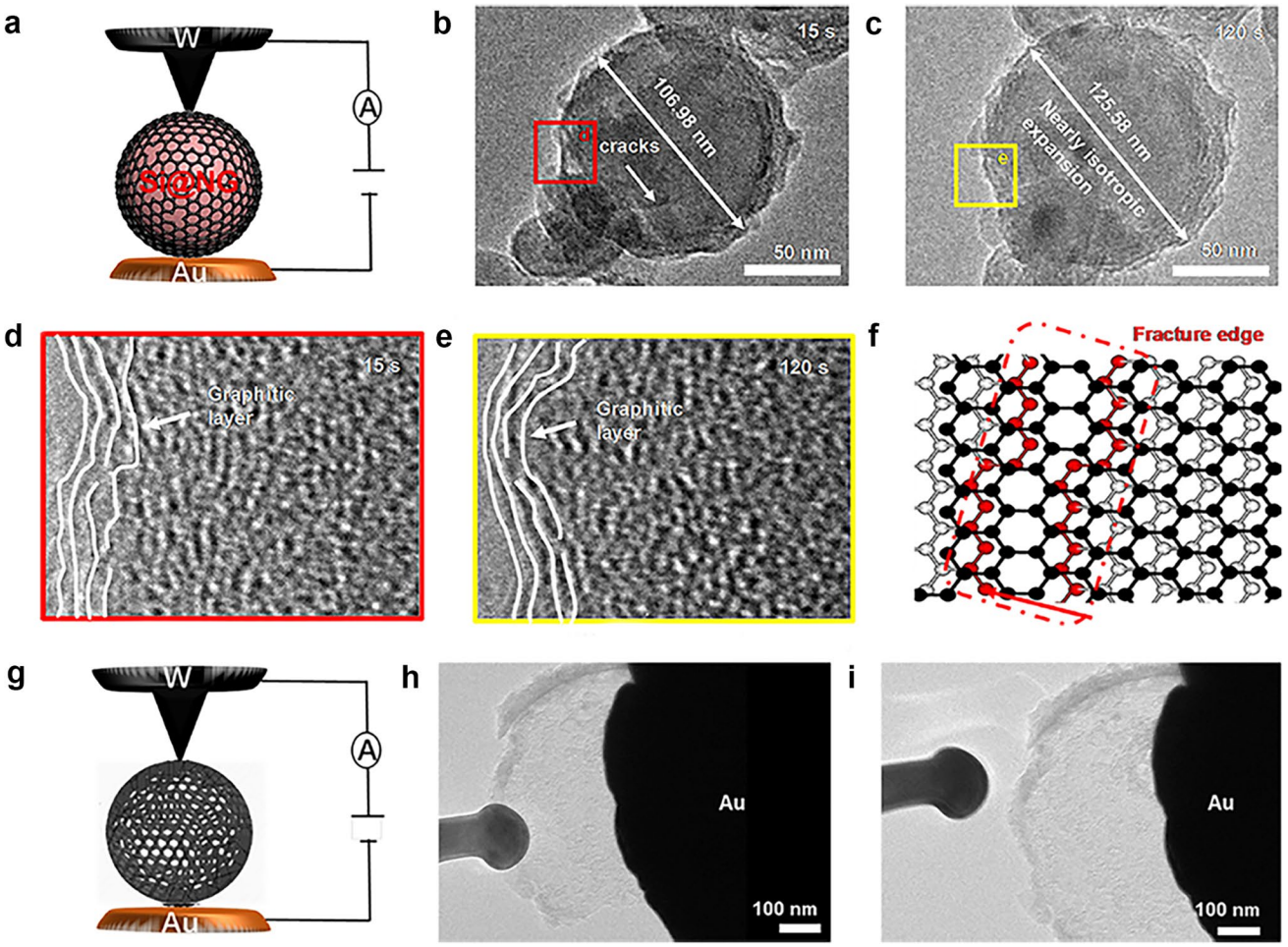

Fig. 6 **a** Simple schematic diagram of in situ TEM. Volumetric changes in a single Si@NG structure at **b** 15 s and **c** 120 s in the discharge process. **d, e** HRTEM pictures of a fracture in the NG shell's inner layer. **f** Illustration of an inner layer fracture and the integrity of the outside layer of the Si@NG NG shell. **g** Schematic representation of N-doped C subjected to in situ TEM test. TEM pictures of an NG shell **h** pushed by a tungsten probe and **i** after pressing [116]. Copyright © 2020, Elsevier

section of the gold wire and slid sideways. However, when the tungsten wire was removed, the coating layer bounced back without complete deformation, indicating that the coating layer exhibited excellent elastic performance and tolerated certain stresses.

3.1.2 X-Ray Tomography

In terms of the Si nano-/microparticle accumulation, cycling instability may occur in different mass directions, which are difficult to determine by using traditional methods and require the destruction of thin samples. The analysis of the failure mechanism owing to phase transitions in the discharge/charge process, particularly for heterogeneous composite materials, presents the same challenge. Moreover, in nanostructured Si anodes, the large surface area facilitates a noticeable SEI in the three-dimensional (3D) pores, resulting in the formation of invalid "dead Si". Tomograms were obtained to follow the structural alterations in the particle distributions associated with the applications. This is because they have a crucial effect on understanding the aging principles of these microscopic structures on a 3D scale.

Recently, synchronized XRT has attracted considerable attention because it enables the visualization of 3D structural variations in Si nanorods during the discharge/charge process. Zhao et al. studied the rapid failure of SiNP anodes and focused on the 3D morphological changes under various periodic capacity conditions to illustrate the root cause of failure [37]. This study presents a new concept for the research and application of nanoalloys as electrode materials. In addition, computed tomography (CT) is a simple time-discrimination technique for identifying the heterogeneity of 3D crystals on large electrodes. Finegan et al. applied a micrometer resolution to study the dynamic process of an Si-graphite hybrid material [117]. The spatial

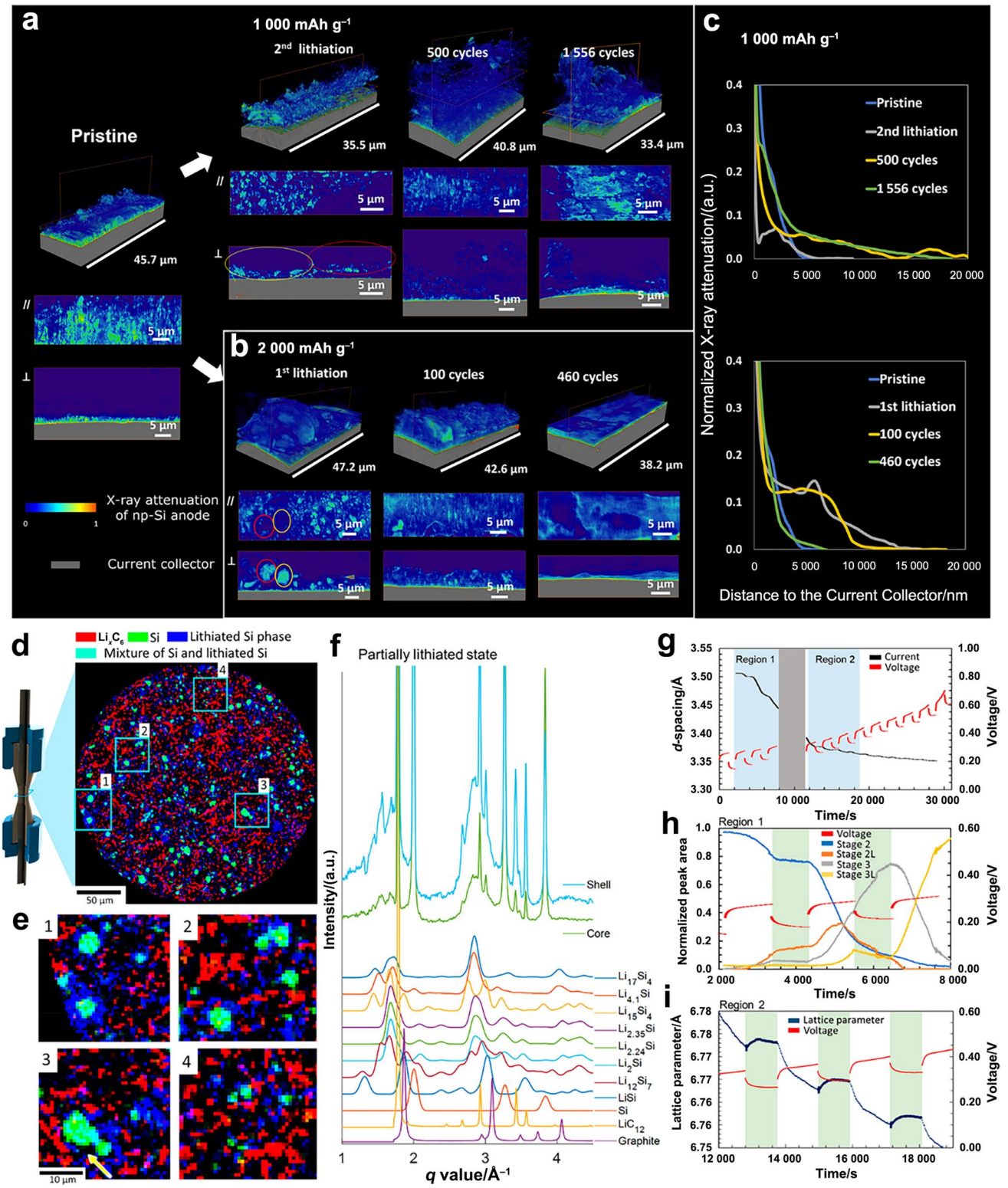

distribution of crystalline Si, Li_xSi, and LiC_{12} was evident, and the presence of Li_xSi indicated that the energy density decreased, resulting in an insufficient battery capacity. In addition, the spatial heterogeneity of single materials (Si and graphite) was confirmed. This suggests that significant progress has been made regarding the spatiotemporal resolution and decomposition of charge during the operation of the electrode particles, which is likely to serve as a foundation for future studies on chemical heterogeneity during cycling.

◂**Fig. 7** X-ray nano-tomography quantified material density 3D visualizations and fictitious cross sections of electrodes cycling in a steady state at **a** 1 000 mAh g^{-1} and **b** 2 000 mAh g^{-1}. **c** Relationship between standardized X-ray absorption and the distance to the current collector. Reproduced with permission from Ref. [37]. Copyright © 2020, Elsevier. Image of an Si-graphite anode taken by using XRD-CT: **d** an XRD-CT slice recorded at the start of the charge process displaying a phase-distribution pattern of crystalline Si (green), Li_xSi (blue), and LiC_{12} (red), where the teal is a blend of green (Si) and blue (lithiated Si) based on complementary color mixing; **e** magnified zones of focus revealing massive Li_xSi phase components in the graphite substrate with crystalline Si centers (1–3) and smaller Li_xSi particles (4). **f** Charge gradient and associated phases. **g** Over operating and open-circuit times, the *d*-spacing corresponds to the (002) reflection of the Li_xC_6 architecture. **h** Magnified time span of Zone 1 demonstrating the incorporated peak regions of the Li_xC_6 phases upon delithiation. **i** Magnified zone of concern displaying the *c*-lattice value of the solid-solution graphite phase over activation and open-circuit (green). Reproduced with permission from Ref. [117]. Copyright © 2019, American Chemical Society

3.1.3 In Situ X-Ray Diffraction

The evaluation of the phase structural variations relied heavily on XRD. These are not confined to thin-film samples and may provide a vast quantity of information on bulk Si materials. Moreover, in situ XRD facilitates extensive analysis of the bulk phase changes in real cells involving liquids with volatile electrolytes, as well as the detection of in situ crystalline transitions at high temperatures. Therefore, in situ XRD is commonly employed to describe LIB transitions during lithiation/delithiation. Furthermore, high loads from high-speed charges introduce stress deformations, which require characterization. In situ XRD can accurately detect stress deformation and residual stress through variations in the diffraction peak, thus revealing a multiphase strain distribution and stress-induced fading mechanism.

The discharging/charging process velocity of the lithium ions varies significantly with the direction of the lithium-ion penetration, with <111> being the least rapid and <110> the quickest. Zhang et al. [118] evaluated the crystalline structure evolution of Si nanoribbons (SiNRs) (Fig. 8a) and SiNPs (Fig. 8b) during initial cycling via in situ XRD. For the SiNRs, the Li–Si alloy exhibited phase transitions resembling those of Si during the discharge procedure. The crystalline plane spacing gradually increased with increasing Li insertion on the (110) surface, which is consistent with the directionally constrained expansion of the SiNRs. The study concluded that restricting the invasion direction of Li^+ in the <110> range was beneficial for retaining the durability of the atomic order. In contrast, the new SiNP peak of the Li–Si alloy exhibited an amorphous structure and relative homogeneity. No clear angular shifts or maximum Si peaks were observed. In addition, in situ TEM experiments were conducted to further analyze the dynamics of the discharging/charging process. As shown in Fig. 7c, the maximum thickness and width of the SiNRs were 17 and 168 nm, respectively. When in close contact with Li, the Li ions rapidly diffused into the SiNRs with a significant increase in thickness (Figs. 8c2 and 8c3). At 40 s, the thickness and width of the SiNRs increased to 43 and 182 nm, respectively (Fig. 8c4). Therefore, during the discharging process, the SiNR first expanded along the *t*-axis and then retained its original thickness along the *l*- or *w*-axis. During the charging process, the SiNR shrunk uniformly, and the thickness decreased from 43 to 28 nm (Figs. 8c5–8c8). The change in the crystal structure of SiNR during the (de)lithiation procedure further elucidated its excellent cycle durability and provided a useful concept for the study of other alloy-based anode materials.

3.1.4 In Situ Raman Spectroscopy

Because Raman spectroscopy is sensitive to symmetric structures, the structural revolution of electrode materials related to voids, defects, and phase changes can be demonstrated. In addition, Raman spectroscopy can be used to study low-crystallinity amorphous composites without a neat arrangement of long-distance structures, making it superior to XRD. For instance, Si and Li_xSi can be observed as amorphous forms during the discharging/charging process.

Zhou et al. studied the discharging/charging process of Si-Ge electrode materials using in situ Raman spectroscopy [119]. The Raman signal changes of Si-Ge and Si during the initial lithiation process are demonstrated in Figs. 9a–9c. With the continuous insertion of Li^+, the Raman peak of Ge began to weaken at 0.6 V, and the Raman peak of Si gradually weakened below 0.4 V and almost disappeared at the end. These results show that the alloying lithiation of Ge occurred before that of the Si-Ge composites, and that of the Si anodes occurred below 0.4 V. In contrast, for the Si anodes, the Raman peaks of Si weakened after charging and then gradually became stronger. Nevertheless, the Raman peak was still observed until the end of the discharge, indicating that the conductivity and ion diffusion of Si were lower than those of the Si-Ge composites. Therefore, the Ge additives could reduce the Li potential barrier of Si, thereby improving the stability of the Si anode cycle.

Wang et al. elucidated the growth of SEIs using in situ Raman spectroscopy [120]. The Raman peaks located at 1 090 and 1 097 cm^{-1} are attributed to CO_3^{2-}, which may be due to the radical polymerization (Fig. 9d). The fluoroethylene carbonate (FEC) and ethylene carbonate (EC) first reacted with the FEC-containing electrolyte before radical polymerization and discharged below 1.3 V. The intensities of these two Raman peaks increased significantly and then remained relatively unchanged with decreasing potential, indicating SEI growth at higher voltages. The corresponding mapping (Fig. 9e) depicted the changing trend.

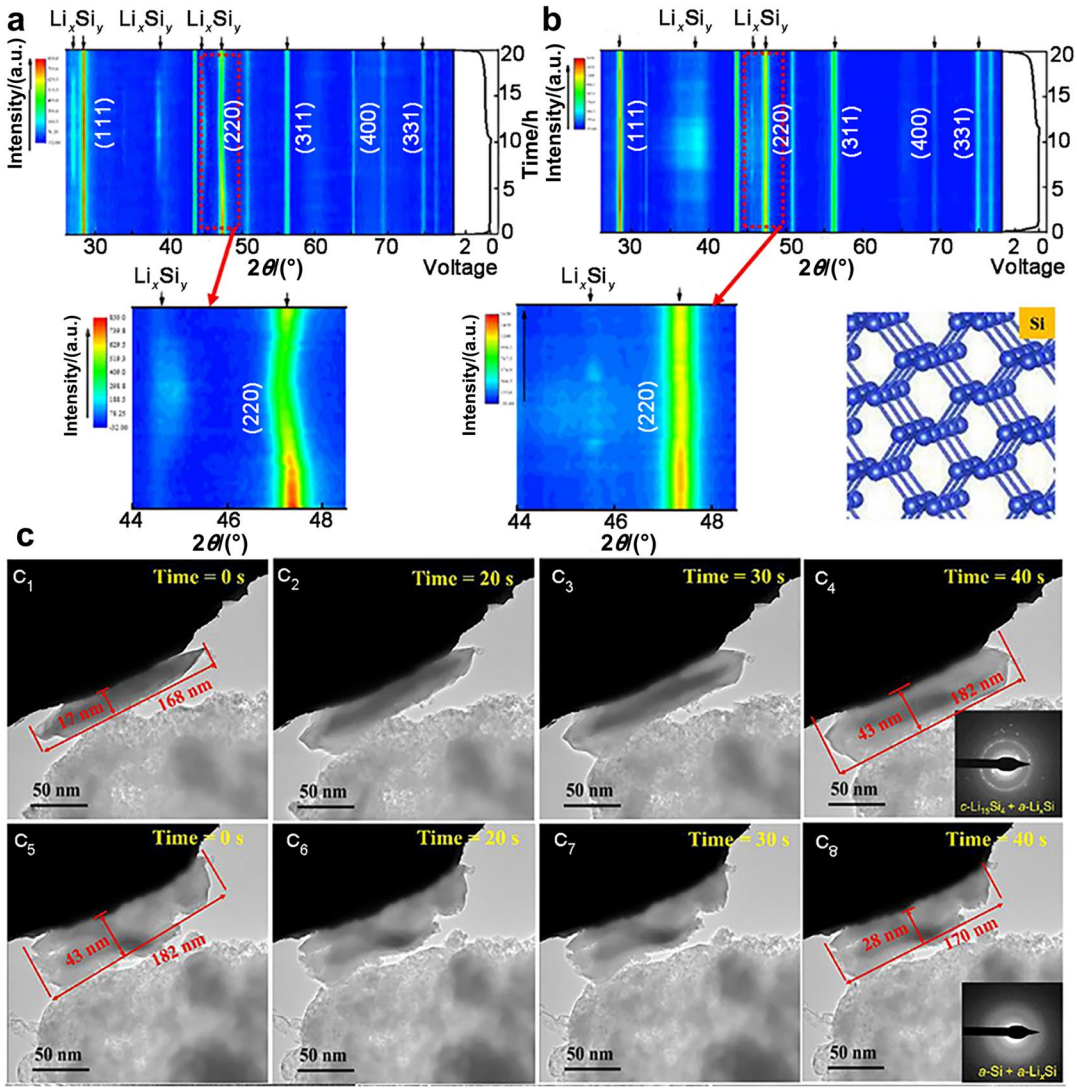

Fig. 8 **a** Si nanoribbon and **b** SiNP anode structure development in two-dimensional contour plots of in situ XRD during the initial (de) lithiation at C/10 in a half cell. **c** Consecutive in situ TEM images depicting the SiNR discharge procedure at 0, 20, 30, and 40 s, respectively, and the SiNRs' delithiation process at 0, 20, 30, and 40 s, with modification. Reproduced with permission from Ref. [118]. Copyright © 2021, Elsevier

3.1.5 In Situ Atomic Force Microscopy

In terms of multiple microscopic techniques, atomic force microscopy (AFM) has a high resolution and high surface sensitivity. Advancements in AFM technology have accelerated the study of Si anodes, particularly the volume evolution, with the aid of the instantaneous visualization of structures in three dimensions.

For most Si-based anode materials, the volume expansion during cycling is the main failure mechanism; however, the electrochemical-mechanical coupling behavior remains unclear. Liu et al. applied in situ AFM to monitor real-time morphological changes in micro-Si (μSi) (Fig. 10) [121]. In addition, the significant mechanical evolution of the electrode materials was successfully visualized, including the early comminution, initiation and patterning of cracks, irreversible volume changes, formation of a fresh SEI at the crack surface, and particle insulation. Moreover, in situ AFM has demonstrated that limiting the limiting voltage, such as 0.7 V versus Li/Li^+, can suppress the mechanical defects at the μSi anodes and improve the capacity stability by reducing the battery impedance. These results prove that in situ AFM has potential for the application in monitoring the electrochemical mechanical behavior of a variety of electrode materials in the "real-world" electrode level.

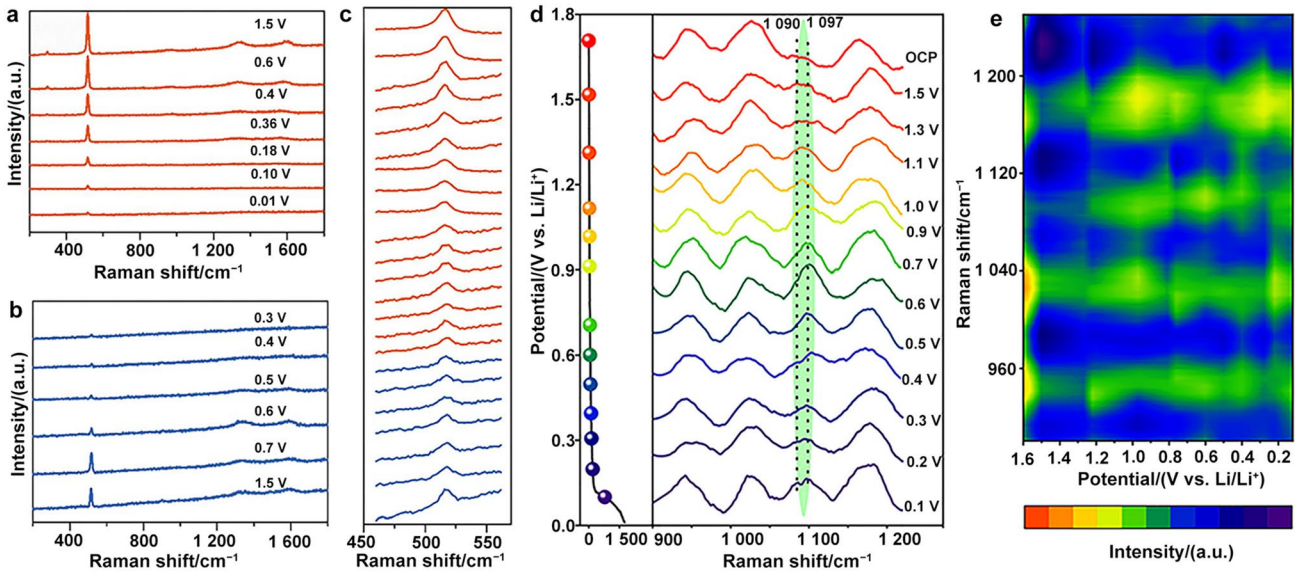

Fig. 9 In situ Raman spectra of Si-Ge in **a** lithiation process and **b** delithiation process and **c** corresponding enlarged images (the orange, discharge; the blue, charge). Reproduced with permission from Ref. [119]. Copyright © 2019, Royal Society of Chemistry. **d, e** In situ Raman spectra and mapping of Si@$MoSe_2$ throughout the (de)lithiation procedure. Reproduced with permission from Ref. [120]. Copyright © 2022, American Chemical Society

3.2 Characterizations of Chemical Composition

With the rapid development of surface sensing methods such as photoelectron energy spectroscopy and secondary ion mass spectroscopy, the surface makeup of electrode materials can potentially be evaluated. Quantitative measurements of the electrode material and electrolyte composition have also been taken possible by using bulk-level techniques including nuclear magnetic resonance (NMR), diffraction spectroscopy, and absorption spectroscopy. Typically, these detection techniques are used in conjunction in laboratories. Furthermore, the use of recently created high-energy sources enables a more in-depth analysis and dynamic tracking of batteries. Using these characterization approaches, researchers studying batteries can evaluate the enhancement caused by the material modification and cycling instability linked to the compositional augmentation of anodes and electrolytes.

3.2.1 Hard X-Ray Photoelectron Spectroscopy

X-ray photoelectron spectroscopy (XPS), which has been widely used to examine electrode-electrolyte interfaces, is the foundation of a novel method referred to as hard X-ray photoelectron spectroscopy (HAXPES). However, the frequent generation of dense SEI with repeated cycling makes it difficult to evaluate the bulk Si material beneath the SEI in Si anodes. An external Si-oxide coating that mitigates the XPS response and hinders the evaluation of the Li_xSi alloying procedure is often present when the growth of a thick SEI film is related to the formation of Li_xSi. Given that high-energy photons can provide further details regarding the exterior and evaluate tightly bound essential electrons, such as Si 2p, this HAXPES technique has been proposed to fully identify the cyclic properties linked to SEI formation and Li_xSi alloying.

Electrolyte components can affect the cycling properties related to SEI development in Si-based LIBs. HAXPES is currently used to examine the impact of various solvent salts on lithiation/delithiation; Li_xSi production may also be examined in future studies [122]. The Si anode can retain approximately 1 200 mAh g^{-1} for 100 cycles with this electrolyte composition. Extended cycling resulted in an increase in the SiO_x content and a reduction in the silicon particle size. This electrolyte and its breakdown products do not cause any adverse side effects on the active Si material, unlike $LiPF_6$-based electrolytes. These findings confirm the benefits of SEI-generating compounds. Polycarbonates and significant LiF concentrations in the SEI are preferable to other carbonates created by the breakdown of EC and dimethyl carbonate (DMC). This research demonstrates that LiTDI is a promising salt for Si anodes when combined with the examined additives. The spectra with cross-linking characteristics obtained using the HAXPES technique effectively show how the electrolyte species may alter the cycling stability and assist in the creation of new electrolytes for Si-based LIBs.

For Si-based anodes, the cycling stability primarily relies on binders because a robust binder can prevent the

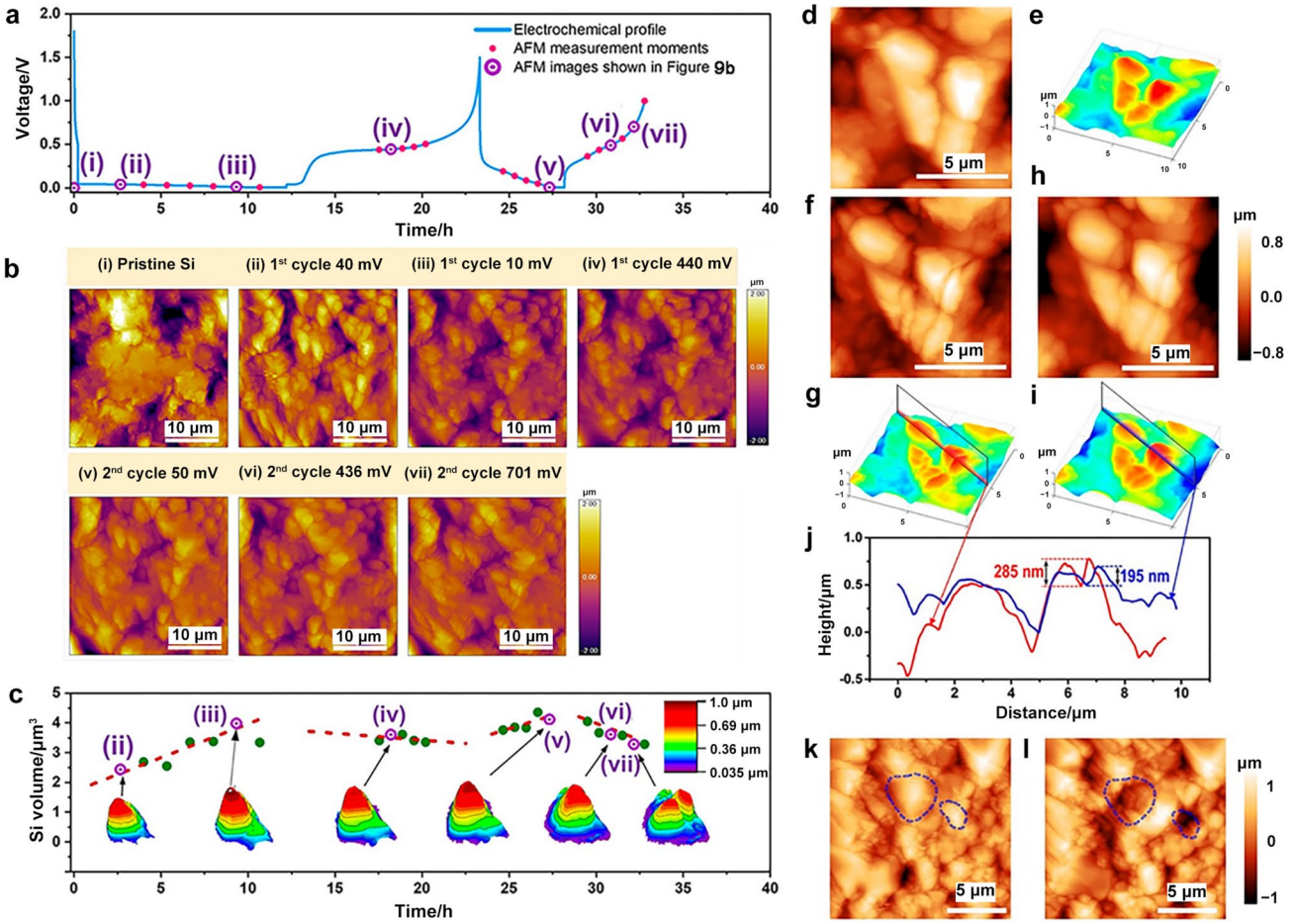

Fig. 10 **a** Pattern depicts the voltage profile acquired from the in situ AFM half-cell for the first two cycles. **b** In situ AFM pictures were captured throughout the first two (de)lithiation processes (i–iii). **c** Pattern depicts a 3D representation of a typical Si particulate and its volumetric variations from (ii) to (vii). The transformation of Si particle contacts: cross-sectional height measurements and 3D visualized images were collected **d, e** before crack development, **f, g** immediately following fracture generation, and **h, i** after resting for 2 h. Reproduced with permission from Ref. [121]. Copyright © 2022, American Chemical Society

pulverization of SiNPs, leading to electrical isolation. To learn more about the effect of binders in the substrate material on the early development of the SEI layer, Young et al. performed HAXPES on new electrodes, cycled at a lower voltage, or cycled completely [123]. To determine the modifications to the SEI that occurred after the initial creation, they also examined the electrodes that were cycled 5, 10, and 20 times. Moreover, they estimated the thickness of the SEI based on the number of cycles, showing that polyacrylic acid (PAA) formed the weakest SEI, followed by carboxyl methyl cellulose (CMC)-PAA, CMC, and polyvinylidene fluoride (PVDF) to increase the layer thickness.

3.2.2 Time-of-Flight Secondary Ion Mass Spectroscopy

Time-of-flight secondary ion mass spectrometry (TOF-SIMS) was used to measure the percentages of various ions (exact parts per million) using small quantities of secondary ions drawn from the sample surface. Utilizing its sensitivity to Li signals, TOF-SIMS can also be used to evaluate Li-Si discharging/charging processes. The cause of cyclic deterioration in Si anodes requires further study. In addition to cyclic mechanical destruction, the interfacial chemistry (such as the Li^+-consuming process) should be considered when analyzing the SEI stability. Owing to the difficulty in monitoring lithium species and microscopic activity, such research continues to encounter obstacles. TOF-SIMS was used in this context to determine the SEI generation reactions linked to the Li-involved process and to decipher its relevance in evaluating these reactions.

Electrolyte components can impact the cycle behavior involved in the SEI development of Si-based LIBs, and a small quantity of water in the electrolyte is one of the elements that is unfavorable for the electrochemical properties. However, attempts to stabilize SEI for better electrochemical properties have been hindered by insufficient expertise

on the basic and mechanical concepts of SEI generation, development, and characteristics in the absence of water. Therefore, Ha et al. used TOF-SIMS to evaluate the SEI established in a Gen2 electrolyte (1.2 mol L^{-1} $LiPF_6$ in ethylene carbonate/ethyl methyl carbonate, 3:7 by weight) with and without additional water (50 μmol mol^{-1}) at different voltages [59]. The SEI exhibited either potential- or liquid-concentration-related variations in the shape and chemical content. Excess water in the electrolyte led to disruptive reactions that began at approximately 1.0 V and ended with a reduction in the constituent parts of the electrolyte and the formation of an insulating fluorophosphate-rich SEI. Furthermore, $LiPF_6$ degradation produces hydrofluoric acid, which interacts with the surface oxide layer of the Si electrode to produce a scarred and irregular SEI structure.

Moreover, a steady interface between the Si electrodes and electrolytes is crucial for achieving outstanding electrochemical performance in LIBs. Ha et al. used molecular layer deposition (MLD) to deposit a Zn polymer layer on an Si anode, which acted as an artificial SEI [124]. TOF-SIMS was used to evaluate the effect of the zincone coating on the structure and thickness of the SEI. The Si@10-ZC anode exhibited a lower SEI than the basic sample (> 300 s). This may have been the cause of the Si@10-ZC electrode's decreased SEI resistance of R_{SEI} (Figs. 11a and 11b). In addition, the ZnO^- signal was consistent underneath the SEI, showing that metallic zinc was uniformly distributed throughout the basic sample. The poor Si signal in Fig. 11c suggests that the SEIs covered the surface of the Si@10-ZC anode. Figure 11d shows the Si signal attaining saturation after 220 s of sputtering, suggesting that Si was entirely illuminated. Metallic zinc was equally dispersed throughout the electrode. Remarkably, LiF shows scattered accumulation, which may be attributed to its porous structure. The resulting 3D reconstructions (Fig. 11e) clearly show the electrode structure. Metallic zinc was spread equally across the electrode, similar to columnar LiF. This pattern of dispersion is essential for increasing the electron/ion transport in Si electrodes.

3.2.3 X-Ray Absorption Near-Edge Structure Spectroscopy

X-ray absorption near-edge structure (XANES) can be used to assess the oxidation state, site symmetry, and covalent bond forces of an intended component. As a result of this characterization, we can evaluate the chemical bonding states linked to the compositional alteration of the electrode materials, which is important for evaluating the battery capacity and cycling stability [125].

XANES was used to identify the bonding changes related to cyclic deterioration in the silicon monoxide (SiO) hybrid anodes. Xu et al. established a simple and low-cost method for producing an in situ graphene-coated SiO anode utilizing coal-derived HA and employed STXM and XANES spectra to evaluate the shape and chemical content of P-SiO with D-SiO@G particulates [126]. The Si-atom-sensitive structure of the cycled particles, obtained by combining STXM image sequences at the Si K-edge, is shown in Figs. 11g (P-SiO) and 11i (D-SiO @G). The concentrations of the anode materials and SEI constituents in D-SiO@G and P-SiO were chemically mapped by matching the STXM stack with the Si K-edge XANES spectra, and the conclusions are shown in Figs. 11h and 11j, respectively. Analyses revealed that these two components were spatially separated in both samples. P-SiO (Fig. 11j) contains more nonanode particle Si-containing species than D-SiO@G (Fig. 11h), implying a more unstable SEI layer. These findings suggested that the graphene layer accelerated the development of a robust SEI layer during cycling. The Si K-edge XANES spectra of bulk P-SiO and D-SiO@G (the red in Figs. 11h and 11j) and the SEI of P-SiO and D-SiO@G are depicted in Fig. 11k (the green in Figs. 11h and 11j). The XANES adsorption peak at 1 840 eV was assigned to the Si phase, whereas that at 1 847 eV was ascribed to oxidized Si, including SiO_2 and Li_2SiO_3. Figure 11l shows the identification of Li_2CO_3, a durable SEI, in the carbon-based anodes using O K-edge XANES spectra and STXM images of the cycled D-SiO@G anodes. This advanced D-SiO@G electrode could retain approximately 1 937.6 mAh g^{-1} at 0.1 A g^{-1} with an initial Coulombic efficiency (ICE) of 78.2%. These new XANES findings are expected to aid researchers in having a better understanding of the causes of instability in Si-based anodes.

3.2.4 Synchrotron Radiation Spectroscopy

A powerful synchrotron radiation light source (SRL), with constantly changing wavelengths, exceptional intensity, and resolution, has promoted detailed research on the local biochemical and geometrical conditions in materials. Advancements in synchrotron radiation have enabled a comprehensive and high-quality analysis of the components of electrode materials. As noted previously, the components across the electrode in Si-based LIBs can interact during the lithiation/delithiation process, complicating our understanding of the failure mechanism. Considering this, synchrotron radiation photoelectron spectroscopy (SRPES) has been applied, which enables continuous and detailed profiling of the electrode makeup at tunable photon energy. SRPES has been used to evaluate the electrode surface reactions caused by passive materials in Si anodes during aging.

Jeschull et al. demonstrated the rapid transformation of a native SiO_x coating into hazardous SiO_xF_y in Si anodes created from a sodium carboxymethyl cellulose (CMC-Na) binder and acetylene black (AB) or ketjen black (KB) [127]. This study deduced that adverse surface reactions

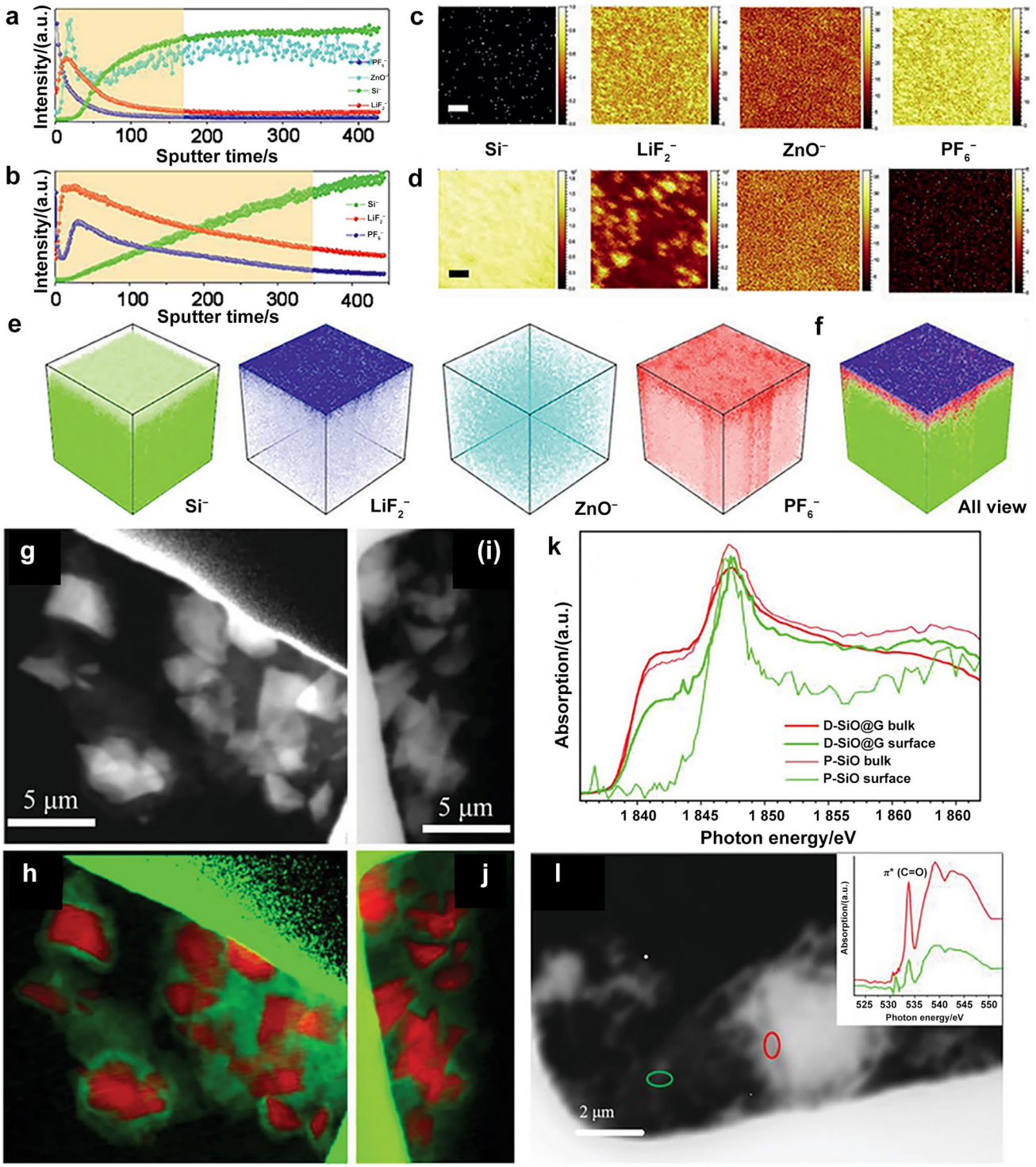

Fig. 11 Depth pattern of several secondary ion species obtained by sputtering: **a** Si@10-ZC electrode and **b** blank sample. TOF-SIMS patterns of Si@10-ZC anode after sputtering for **c** 20 s and **d** 220 s. **e, f** Approximate volume reconstructed versions in three dimensions that correlate to the depth profiles. Reproduced with permission from Ref. [124]. Copyright © 2021, Wiley-VCH. Architecture of **g** P-SiO and **i** D-SiO@G after 50 cycles and **h, j** corresponding chemical mapping, respectively. **k** Si K-edge XANES spectra of the four samples. **l** Morphology of cycled D-SiO@G particles and corresponding selected regions mapping, with modification. Reproduced with permission from Ref. [126]. Copyright © 2021, Wiley-VCH

caused rapid deterioration and unsatisfactory comprehensive properties of KB-based electrodes. Owing to the preservation of CMC-Na, traditional AB-containing anodes retain a large portion of their SiO_x coatings. SRPES can probe valence states and hydrogen bonds with a high resolution and is an effective approach for exposing the fading process related to the development of surface components. Furthermore, Hirata et al. observed Si-containing architectures in extremely disorganized and homogeneous SiO components using both local and global data, adding necessary proof that a-SiO suffers from dispersion by producing Si- and Si-dioxide-like zones [128]. Owing to its distinguished capacity to perceive Si oxidation states, synchrotron HEXRD supports compositional evaluations and increases our understanding of the chemical mechanisms underlying its electrochemical properties.

3.2.5 Solid-State Nuclear Magnetic Resonance Spectroscopy

Nuclear magnetic resonance (NMR) technology offers substantial chemical information because of its susceptibility to localized short-range material architectures. NMR analysis is widely employed to study electrodes and electrolytes because it can be used for both bulk and liquid materials. Furthermore, it is possible to ascertain the chemical constitution of the SEI and binder, including the organic substances and Li compounds produced during the lithiation/delithiation process, which depends on the influence of particular local environments on the chemical shift of the characteristic peak.

NMR can demonstrate the discharging/charging process of Si anodes, which involves crystallized-to-amorphous phase transitions. The Li-Si configuration assessment is crucial for battery advancement because the evolution from crystalline Li_xSi to amorphous Li_xSi, which is frequently observed in the lithiation process, may result in capacity loss. The short-range structural evolution that occurs during the discharging/charging process may be difficult to discern from the diffraction patterns, owing to the amorphous nature of Li_xSi. Therefore, NMR spectroscopy was used to examine Li_xSi phase transitions. Kitada et al. evaluated the Li_xSi phases that occur during the discharge (charge) of SiO and compared their findings with those of a pristine Si electrode [129]. When lithiating a-SiO with a considerable Li amount at $x = 3.4–3.5$, in situ ^{7}Li and ^{29}Si solid-state NMR coupled with a thorough electrochemical study revealed that a distinctive metal-based Li_xSi phase is formed/decomposed by means of an uninterrupted structural change related to the amorphous states that vary in their level of Si-Si interaction (Figs. 12a–12d). In contrast with pristine Si electrodes, which create the final component crystalline $Li_{15}Si_4$, the structural history differs via a double-phase procedure. In contrast, the dimensions of the structured Si domains in pure SiO determine the reaction pathway. A phase resembling $Li_{15}Si_4$ occurred in a matrix of SiO_2 when crystalline domains larger than 3 nm were present, although this phase had a higher overpotential. The constant formation/decomposition of amorphous Li_xSi components lacking hysteresis, with the phase shift related to the synthesis of c-$Li_{15}Si_4$ and the partially electrochemically activated SiO_2/Li_xSi buffering layer, is required for the a-SiO cycling performance.

3.2.6 Cryo-TEM

Although traditional TEM can produce fundamentally precise images of structures, it is unsuitable for SEI analysis because of the chemical reactivity of the SEI layer and its sensitivity to electron beam irradiation. Consequently, most information on SEIs derived through classical TEM is restricted to the micron scale and lacks comprehensive crystallographic structures. Nonetheless, some studies have recently used cryogenic electron microscopy (cryo-EM) to analyze the atomic resolution patterns of SEIs in their original state by freezing the desired object in liquid nitrogen to maintain its initial form.

The instability of the Si electrode SEI has restricted its industrialization; however, this SEI characteristic remains unexamined because of the difficulty in defining the nanoscale passivation layer. Huang et al. used atomic-resolution cryogenic (scanning) TEM [cryo-(S)TEM] and electron energy loss spectroscopy (EELS) to examine the structure and chemistry of SEI, revealing their progression throughout the first cycle [130]. Because of the strong reversibility of the SEI, we observed the genesis of the Si SEI instability in EC electrolytes (Figs. 12e–12h). The involvement of the key electrolyte FEC in extending the cyclability of an Si anode by depositing a magnetically indestructible polyethylene coating on its surface was elucidated. Such studies provide insight into the unreliability of Si anodes in conventional EC-based electrolytes and the impact of additives on the SEI stability.

Zhang et al. employed cryo-TEM to demonstrate SEI development and its interaction with engaged Si during the first discharging/charging process [131]. The findings showed that the SEI occurred electrochemically prior to and throughout Si lithiation and broke down after delithiation (Figs. 12i–12p). It consumed more than 10% of the charge and, when separated from the electrical network, caused the development of inactive Li_xSi. FEC has been observed to be advantageous as an electrolyte additive for creating a largely steady SEI, thereby extending the cycle life. These results provide a thorough understanding of SEI development and explain the relationship between SEI stability and cycling properties.

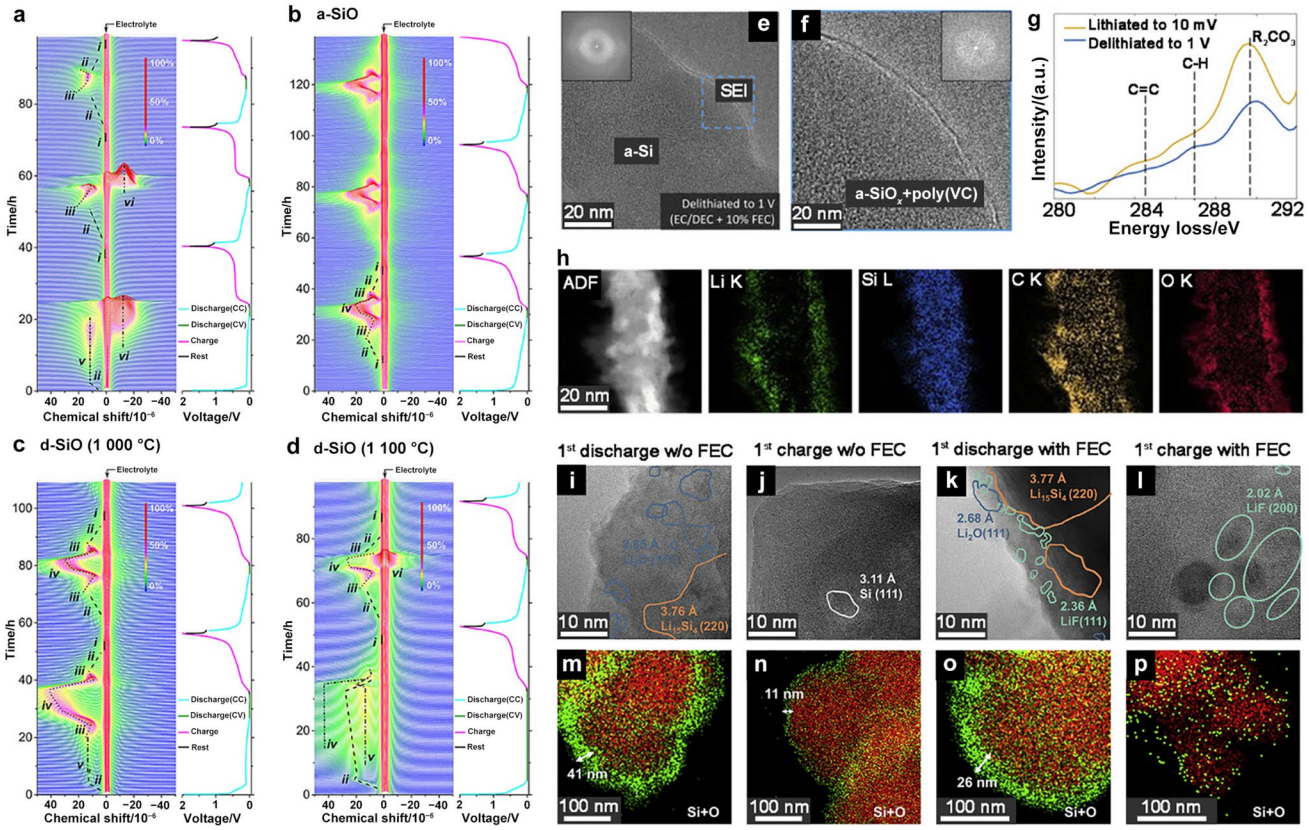

Fig. 12 **a**–**d** ^{7}Li in situ NMR results for four electrodes. Reproduced with permission from Ref. [129]. Copyright © 2019, American Chemical Society. **e** HRTEM image of Si NW during (de)lithiation. **f** Enlarged HRTEM pattern of Si NW SEI. **g** EEL image of the C K-edge from the Si NW during (de)lithiation. **h** Si NW STEM EELS mapping at 1 V delithiation. Reproduced with permission from Ref. [130]. Copyright © 2019, Elsevier. HRTEM with the corresponding EDS images **i, m** after the initial discharge process and **j, n** initial charge process in FEC-free electrolyte, and **k, o** after initial lithiation and **l, p** initial delithiation in the FEC-containing electrolyte. Reproduced with permission from Ref. [131]. Copyright © 2021, Elsevier

Overall, these advanced technologies provide insights into the charging-discharging process and failure modes of Si anodes, promote structural modification, and establish Si-based batteries with cycling stability and long lifetimes. Despite the in situ assessments using techniques such as Raman spectroscopy, AFM, angle X-ray scattering (AXS), and NMR being useful for considering multiple reaction procedures of Si electrodes, more sophisticated characterization techniques and simulation methods should be established to gain a deeper understanding of prospective structural engineering.

4 Design Strategies of High Energy Density Si-Based Electrodes

Currently, research is being conducted on sound engineering of Si-based electrodes to address the significant technical challenges associated with their electrochemical properties. The first part of this section discusses the structural design solutions for minimizing the mechanical stress in high-capacity anodes. Subsequently, an interface engineering strategy for compensating for the capacity loss and increasing the ICE is presented. Finally, novel elastic/conductive binders and electrolyte additions that enhance ion and electron transport kinetics and maintain SEI growth are discussed (Fig. 13 and Table 1).

4.1 Structural Design

As previously reported, the fragile characteristics and poor mechanical behavior of bulk and microsized Si cause cracks and pulverization. Therefore, Si-based nanomaterial anodes with different structures, such as hollow and porous frameworks, have been shown to effectively provide sufficient open space to contain volume changes, thereby alleviating mechanical strain. The following sections describe the manufacturing process and applications of Si anodes [132–135].

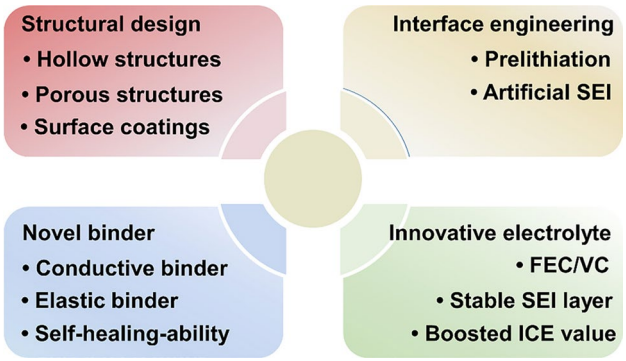

Fig. 13 Widely used methods for enhancing the stability of Si anodes

4.1.1 Hollow Structures

Hollow Si architectures are innovative alternatives for long-lifetime LIB anodes, and their interior void areas can support volume expansion and significant mechanical strain during (de)lithiation. Furthermore, the thin surface layers offer narrow diffusion pathways for Li ions. Considering the aforementioned problems, Zhang et al. demonstrated a narrative-integrated hollow Si/C nanosphere composed of Si and significantly increased the amorphous carbon coating generated by incorporating CO_2 as an ecofriendly carbon source in magnesiothermic reduction to expedite the commercialization of Si anodes [136]. Interconnected carbon chains were formed in the Si intervals because of the reaction involving CO_2 with the abundant Mg vapor and MgO cores. Furthermore, after acid etching of the MgO templates produced in situ, a hollow architecture was achieved (Figs. 14a–14d). The enhanced Li-ion transit and electron transfer kinetics, with the volume butter effects of the hollow design, led to a novel linked Si/C catalyst with excellent electrochemical performance. This novel synthetic approach is cheap, readily scalable, and will likely assist in the commercial deployment of Si/C composites for high-energy LIBs. Recently, our research team produced an interlinked hollow Si/C nanosphere/graphite hybrid for LIBs [137]. The SiO_2 particles were attached well to the graphite interface when polyvinyl alcohol (PVA) was used as the optimal surfactant. After CO_2 was added to the magnesiothermic reduction, a homogeneous distribution of both hollow Si/C nanospheres and graphite within the mixed materials was achieved, implying that the interoperability of the active ingredients was dramatically enhanced owing to the amorphous carbon strategically generated by CO_2, which is essential, with the characteristic eco-friendly carbon substance (Figs. 14e–14h). After 200 cycles, the Si/C anode displayed a supreme electrochemical property (1 065 mAh g^{-1} at 0.1 A g^{-1} after 500 cycles).

Furthermore, the void-preserving SiO_x/C electrode materials are potential candidates for anodes. Nevertheless, the simple and controlled fabrication of the evenly distributed SiO_x and carbon components with adequate space remains a significant challenge. Zhou et al. designed a molecular polymerization technique to create SiO_x/C hollow particles for LIBs (Fig. 14i) [138]. As silicon and carbon precursors, 3-aminopropyltriethoxysilane and dialdehyde molecules were carefully tailored to form hollow polymer spheres (PHSs) via one-step aldimine condensation without a framework or additive. Different PHSs were created by using the cross-linkers terephthalaldehyde, glutaraldehyde, and glyoxal, illustrating the adaptability of the approach. Furthermore, nanocluster-scale homogeneous SiO_x integration of 5 nm in hollow carbon capsids was made possible by the in situ pyrolysis of the PHSs (Figs. 14j–14r). The

Table 1 Summary of the structure regulation and corresponding electrochemical performance of Si-based electrodes reported previously

Electrode material	Structure	Cutoff voltage	[Capacity/(mAh g^{-1})]/[current density/(mA g^{-1})]/cycle number/capacity retention	Refs.
Si/C	Hollow nanospheres	0.01–1.5	730/0.5/200/56.5%	[121]
Si-C	Nanospheres	0.01–1.5	662/0.5/200/65.7%	[122]
SiO_x/C	Porous composites	0.005–2.0	530/0.5/450/80.0%	[123]
p-Si@C	Porous composites	0.01–1.5	1 562/0.1/100/99.0%	[125]
p-CoNC@Si	Hollow porous cubic	0.01–3.0	1 008/0.5/500/83.5%	[126]
GP-Si	A core-shell gradient porous structure	0.01–3.0	1 059/2.0/500/89.6%	[127]
Si@$Ti_3C_2T_x$@G	Dense porous sphere	0.01–1.5	984.9/1.0/800/63.1%	[129]
P-Si/C@C	Porous microsphere	0.01–2.0	708.6/1.0/820/87.1%	[131]
Si@C	Core-shell structure	0.01–1.2	2 514/0.1/360/75.8%	[133]
YS-SiO_x/C@C	Yolk-shell structure	0.01–3.0	770.5/0.5/500/78.2%	[134]
H-SiNS/C	Carbon-coated porous sphere	0.01–1.5	1 040/0.5/500/90.4%	[135]
Si/Li_2SiO_3/C	Core-shell structure	0.01–2.0	1 583/3.0/200/70.2%	[138]
Li/B-SiO_x@C	Carbon-coated	0.01–2.0	1 184/0.5/200/85.4%	[141]

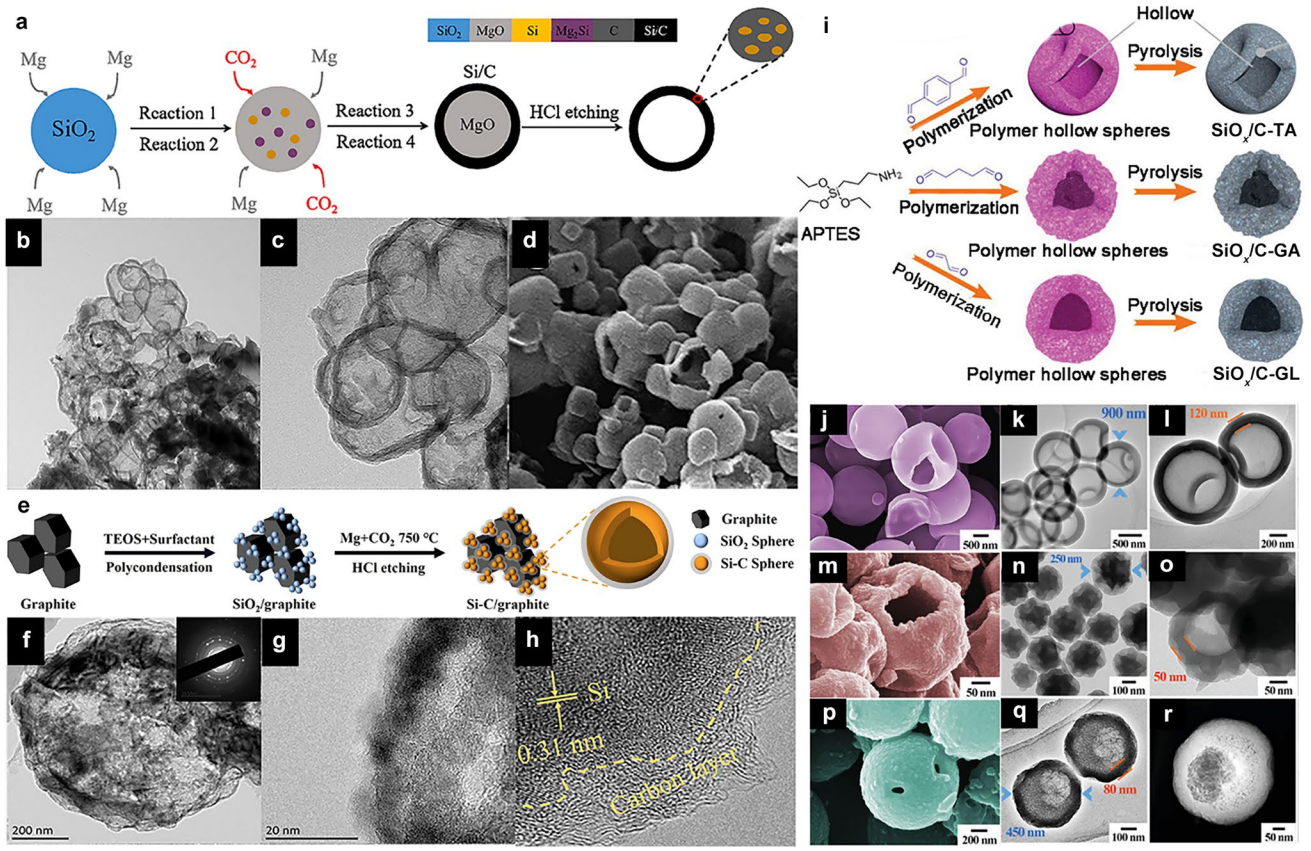

Fig. 14 **a** Scheme of the preparation mechanism of Si/C hollow structures. **b, c** TEM and **d** HRTEM patterns of Si/C electrode materials. Reproduced with permission from Ref. [136]. Copyright © 2021, Elsevier. **e** Scheme of hollow Si-C/graphite composites. **f** TEM and **g, h** HRTEM patterns of Si-C/G-A electrode materials. Reproduced with permission from Ref. [137]. Copyright © 2022, Elsevier. **i** Scheme of SiO_x/C HS (GA, GL). SEM and TEM images of **j–l** SiO_x/C HS-TA, (**m–o**) SiO_x/C HS-GA, and **p–r** SiO_x/C HS-GL with modifications. Reproduced with permission from Ref. [138]. Copyright © 2021. Wiley-VCH

prepared SiO_x/C electrode material exhibited outstanding electrochemical properties such as cycle stability, Coulombic efficiency, and rate. These superior characteristics were attributed to the carbon substrate's well-dispersed SiO_x nanostructures and hollow architecture. This molecular polymerization technique enables the controlled production of template-free hollow structures and makes Si-based hollow hybrids practical and scalable anode materials.

4.1.2 Porous Structures

Electrodes with porous Si structures exhibit better cyclability and stabler SEI layers. Meso-/macropores in Si electrode materials, as earlier stated, were successfully observed to offer open regions for variation without cracking or pulverization [139]. Furthermore, the pores are naturally linked and offer rapid diffusion pathways for Li^+ to penetrate the electrolyte. These benefits provide porous Si anodes with outstanding electrochemical performance. In contrast, the large number of meso-/macropores in bulk Si materials diminishes the gravimetric and volumetric energy densities. Template-assisted methods are often used to create porous Si structures that are then etched or reduced. Etching or reduction is possible without the use of a template.

Liu et al. presented an advanced preparation technique by prolonging the widely used Mg thermal reduction technique for the production of porous Si/C structures (p-Si@C) with interrelated conductive networks and a hierarchical mesoporous framework, conferring it with a satisfactory structure and characteristics (Figs. 15a–15c) [140]. Detailed characterization using numerous methods in conjunction with DFT calculations showed that the p-Si@C nanoarchitecture stabilized the SEI, enabling fast Li^+ electron diffusion. This Si@C anode had a significant electrochemical performance of 1 078.68 mAh g^{-1} at 1 A g^{-1} after 500 cycles (Fig. 15d). Kim et al. used SiNP-enclosed hollow-porosity N-doped Co-integrated CNTs (p-CoNC@SiX) as anode materials for LIBs (Fig. 15e) [141]. These hollow nanocubic materials were prepared by the simple annealing of various amounts of SiNP-encased Zn/Co-bimetallic

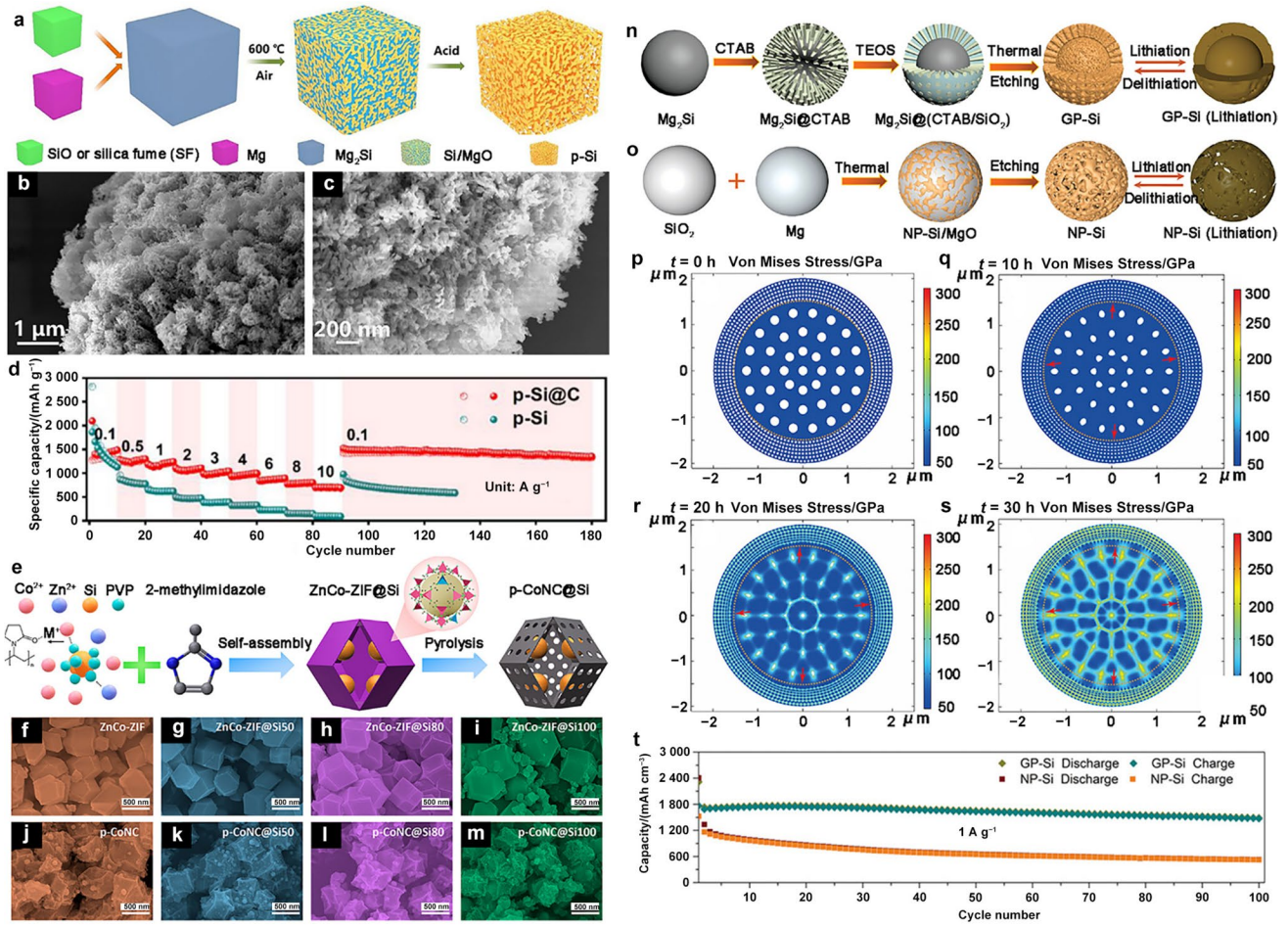

Fig. 15 **a** Scheme of the design and synthesis procedure and **b, c** SEM images of p-Si. **d** Rate behavior of the p-Si and p-Si@C anodes. Reproduced with permission from Ref. [140]. Copyright © 2021, Elsevier. **e** Scheme of the design and synthesis of the hollow porous p-CoNC@Si*X*. SEM patterns of **f** ZnCo-ZIF, **g** ZnCo-ZIF@Si50, **h** ZnCo-ZIF@Si80, **i** ZnCo-ZIF@Si100 before pyrolysis, **j** p-CoNC, **k** p-CoNC@Si50, **l** p-CoNC@Si80, and **m** p-CoNC@Si100 after pyrolysis process. Reproduced with permission from Ref. [141]. Copyright © 2022, American Chemical Society. Preparation of **n** GP-Si and **o** NP-Si. Von Mises Stress distribution and volume change for GP-Si **p** before discharge, and at discharge times of **q** 10 h, **r** 20 h, and **s** 30 h (full discharge), with modifications. **t** Volume-specific capacity of two samples. Reproduced with permission from Ref. [142]. Copyright © 2021, Wiley-VCH

zeolitic imidazolate structures (ZIF@Si) to obtain self-sacrificial frameworks (Figs. 15f–15m). This study presents a unique perspective on the fabrication of highly reversible Si-based anodes for rechargeable LIBs.

Furthermore, the durability and tap density of Si materials are often reduced by the traditional porous architectures. Si has a high melting point and stable chemical composition; thus, few methods are available to manufacture porous structures. A technique for creating core-shell graded porous Si with a robust core and a high-porosity layer was reported by Yang et al. [142]. This massive volume-change strain can be mitigated using a high-strength core. Its rich porous nature guaranteed the continual survival of the SEI (Figs. 15n–15s). This Si anode had a significant electrochemical performance of 1 059 mAh g^{-1} at 2 A g^{-1} after 500 cycles (Fig. 15t). Three appealing characteristics exist in the core-shell graded porous architecture. (I) The porous structure of the shell provides sufficient room for Si to expand in volume during the discharge (charge) process, maintaining the stability of the SEI. (II) The improved Li^+ transmission efficiency of the gradient pore structure was largely due to the increased porosity of the shell.

4.1.3 Surface Coatings

A viable approach to address these limitations is the construction of nanostructured silicon surfaces (yolk-shell, core-shell, and composite materials). Surface coatings are currently demonstrated to be effective in eliminating the immediate contact between Si and the electrolyte, preventing SEI formation, allowing Li ions and electrons to move quickly, and decreasing the mechanical stress induced by

volumetric changes. Si nanostructures have been coated with a range of substances such as carbon, graphene, a series of polymers, metallic substances, and metal oxides. The surface engineering of Si anodes using various techniques is discussed in detail in the following sections.

Carbon Coating Owing to its capacity to enhance electrical conductivity and dampen variations in the Si volume, carbon is extensively utilized as a covering material [143–146]. It has been proven that encasing Si particles, nanorods, and nanosheets in a uniform carbon layer enhances electrochemical performance. Typically, polymers that carbonize, such as polydopamine or polyaniline, are used to cover the surfaces of Si nanostructures [147]. For example, a hydrothermal technique was used to create submicron core-shell Si@C interlaced with carbon nanowires (CNWs) and graphene nanosheets [148]. This Si anode had a significant cycling stability of 1 548 mAh g^{-1} at 0.1 C after 360 cycles. The authors conducted COMSOL Multiphysics and MD simulations to determine the volume expansion during lithiation. The findings showed that lamellar-micron silicon could produce a steady reversible capacity of more than 2 100 mAh g^{-1}, which was in good agreement with the experimental findings. Additionally, Luo et al. suggested an elaborate plan for creating a yolk-shell structure to improve electrochemical performance of the silicon oxide-based anode (Fig. 16a) [149]. Organosilicon nanoparticles were created by hydrolyzing a silane coupling agent, followed by self-condensation. A one-step carbonization process was used to create an SiO_x/C@C composite with a yolk-shell structure (YS-SiO_x/C@C), which was combined with polydiallyldimethylammonium bromide manipulation and a polymeric methacrylate layer (Figs. 16b–16e). This pyrolysis method may effectively ease the volume fluctuation of the SiO_x electrode owing to modification with polydiallyldimethylammonium

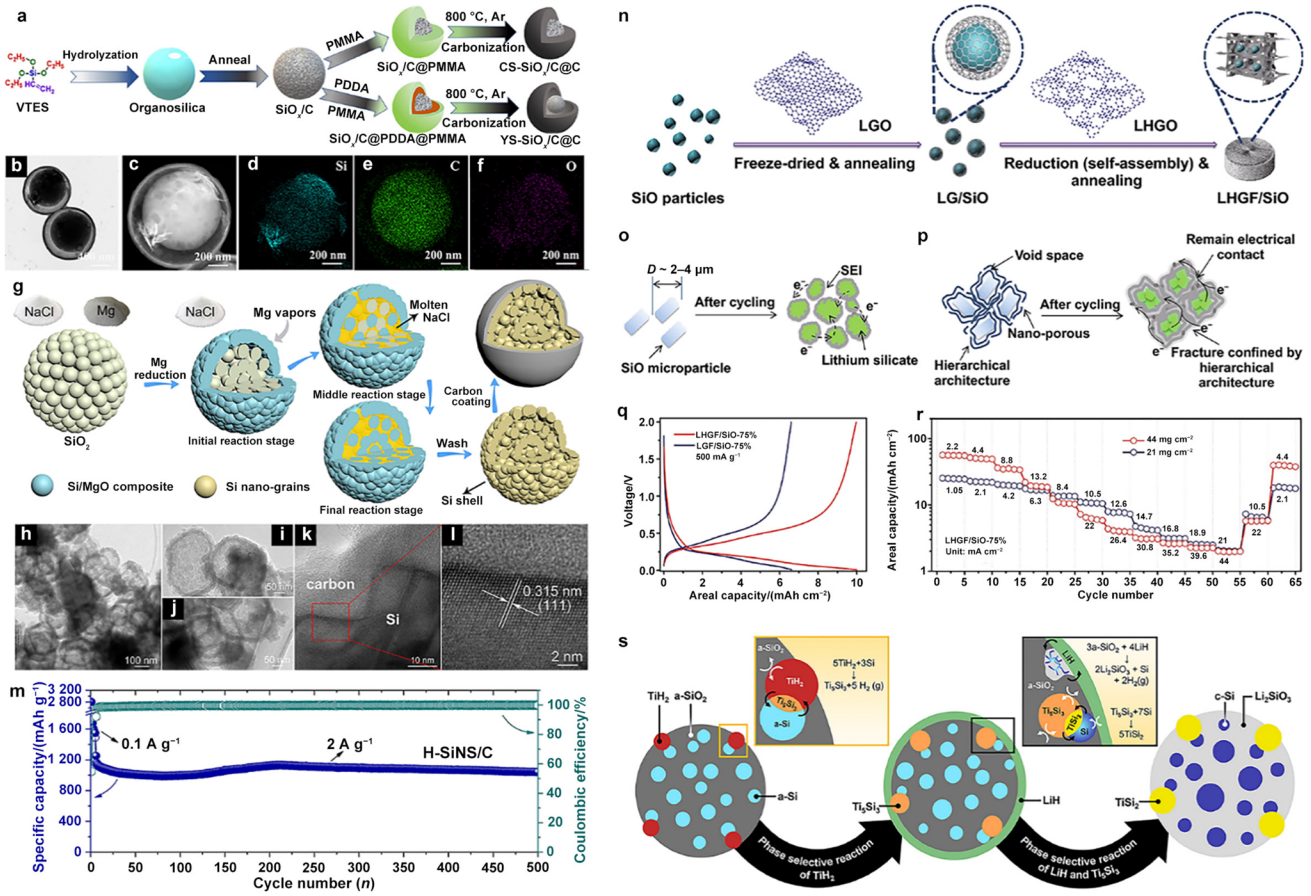

Fig. 16 **a** Synthesis process for SiO_x/C@C composites with different structures; **b** TEM, **c** HAADF pattern, and **d–f** corresponding EDS mapping for YS-SiO_x/C@C electrode. Reproduced with permission from Ref. [149]. Copyright © 2022, American Chemical Society. **g** Scheme of synthesis process for H-SiNS/C material. **h–j** TEM, **k, l** HRTEM, and **m** cycling property of H-SiNS/C material. Reproduced with permission from Ref. [150]. Copyright © 2022, Wiley-VCH. **n** Synthesis procedure of LHGF/SiO materials. Scheme of the structural change in **o** pristine SiO anode and **p** LHGF/SiO anode. Reproduced with permission from Ref. [158]. Copyright © 2022, Springer Nature. **q** Galvanostatic charge/discharge plots of the two electrodes. **r** Rate behavior of LHGF/SiO-75% anode. **s** Scheme of SiO with two different metal hydrides (TiH_2 and LiH). Reproduced with permission from Ref. [159]. Copyright © 2022, Elsevier

chloride, and the carbon coating could boost the overall conductivity. Consequently, the YS-SiO_x/C@C electrode demonstrated exceptional electrochemical properties (770 mAh g^{-1} after 500 cycles, 0.5 A g^{-1}). The findings of this research will aid in the fabrication of materials for yolk-shell electrodes and the progress of outstanding-durability SiO_x electrodes.

Entrapping significant amounts of SiNPs in a thin carbon coating is an interesting alternative technique for increasing the tap density while enhancing the cycle stability, alongside the previously proposed elaborate architectures. For instance, An et al. demonstrated the large-scale fabrication of an intriguing micro/nanostructured pore-rich Si/C microsphere formed by SiNPs securely immobilized onto a micron-sized interconnected C framework covered with a thin C coating (P-Si/C@C) [133]. This P-Si/C@C hybrid had considerable porosity, offering a sufficient tiny interior space to compensate for the massive volume changes in the Si anodes. The thin and sturdy C coating improved the overall structure and rigidity of the SEI. SiNPs placed in a microsized cross-linked C matrix demonstrated outstanding electrical conductivity and structural stability. This P-Si/C@C anode demonstrated exceptional electrochemical properties with a significant discharge capacity of 708.6 mAh g^{-1} after 820 cycles (1.0 A g^{-1}), surpassing the stated findings for Si/C hybrid anode materials.

Double-carbon-shell-coated Si (DCS-Si) nanoparticles have also been fabricated and used as anode materials. Wang et al. prepared a new H-SiNS/C architecture by using a straightforward method (Fig. 16g) [150]. Many small Si nanograins were present in the composite as a tiny mesoporous Si core, which was then covered with a carbon layer (Figs. 16h–16l). During repeated (de)lithiation operations, this mesoporous Si core with extensive tiny inner spaces can efficiently adapt to volume fluctuations and reduce mechanical strain. In addition, the carbon layer can operate as a rigid physical-mechanical buffer to constrain volume changes and ensure structural stability. Consequently, the H-SiNS/C anode exhibited a significant electrochemical performance (Fig. 16m).

Metal/Metal Oxide Coating Coating Si particulates with different metals has been demonstrated to be an effective technique for increasing electrical conductivity, decreasing polarization, and changing the buffer volume [151–153]. An appropriate metal coating should be electrolyte-inert to enable Li^+ penetration into Si. Metal (Ag and Au) and transition metal (Ge, Cu, and Fe) particles are frequently used to replace Si electrode materials. For instance, magnetron sputtering was used to create an Si@Cu composite anode material that was subsequently used in LIBs [154]. The Cu component, which has a greater intrinsic conductivity, significantly increased the conductivity. Compared to the nanomaterials, the irregularly shaped microsized Si particles had a lower agglomeration impact. A carbon layer was added to eliminate the volume impact of the Si electrodes throughout the (dis)charge process, which increased their conductivity and electrochemical properties. The Si@Cu@C anode exhibited significantly improved electrochemical properties (1 130 mAh g^{-1} after 100 cycles). Both processes that were employed to create the Si@Cu and Si@Cu@C anodes can be used for mass production, which is advantageous for achieving reasonable assignments. Furthermore, the magnetron sputtering technology employed for composite powder preparation has numerous applications in the manufacturing of microsized composite materials.

Covering Si anodes with metal oxides is another useful method for improving their electrochemical properties. TiO_2 is a potential coating material owing to its low volume variation (4%), good electrochemical performance, and good thermal properties. Wang et al. created pomegranate-shaped microspheres from SiNPs covered with a TiO_2 coating (Si@TiO_2@rGO) [155]. The anatase phase layer of TiO_2 was more resistant to the structural distortion of Si. After lithiation, the new offspring formed by the TiO_2 coating acted as a fast-speed diffusion channel for Li^+. The porous microspheres offered an adaptable area for Si volume expansion, whereas enveloping the Si@TiO_2 nanoparticles in the flexible graphene decreased the intrinsic tension and increased the conductivity. This layer provided an outstanding electrochemical performance (1 228.7 mAh g^{-1} after 400 cycles at 0.5 A g^{-1}). This study provides an efficient method for promoting the application of SiNPs as anodes in real life.

Hybrid composites 3D Si architectures can intrinsically afford space for volume changes, leading to significantly enhanced electrochemical capabilities for matching Si anodes [156]. Owing to its inherent properties, the volume growth of the SiO_x anode during the cycling procedure could not be prevented. Chen et al. exploited this apparent disadvantage to improve the cycling properties of the SiO_x anodes. $PbZr_{0.52}Ti_{0.48}O_3$ (PZT) was used as an effective inclusion reagent because of the piezoelectric action caused by the SiO_x volume expansion [157]. In particular, significant volume changes may be communicated to the PZT particles, leading to polarization. A piezoelectric potential was created to facilitate the Li^+ movement. A sol-gel technique and high-intensity ball-milling approach were used to create the SiO_x-C/PZT. The SiO_x-C/PZT electrode demonstrated exceptional electrochemical properties, with a remarkable electrochemical performance of 570 mAh g^{-1} after 200 cycles (0.5 A g^{-1}). These noteworthy findings suggest that employing PZT piezoelectric materials can enhance the electrochemical characteristics of SiO_x anode materials. Additionally, this deduction will facilitate the application of PZT and other piezoelectric materials in alloy-based anodes.

Silicon monoxide (SiO) is a fascinating anode material for future-oriented LIBs because of its incredible specific

capacity of 2 680 mAh g^{-1}. Until now, research has been confined with a very modest mass loading (3.5 mg cm^{-2}), severely limiting the areal capacity and its application in commercial systems. The mass loading of such high-capacity electrodes should be maximized to maximize their potential in practical technologies. Zhong et al. proposed 3D monolithic large-sheet holey graphene structure/SiO (LHGF)/SiO electrodes (Fig. 16n) [158]. They developed LHGF exhibited super elasticity and excellent mechanical resilience by employing large-sheet holey graphene building blocks, which are critical for absorbing the significant volume variation of SiO and preserving its structural integrity even under ultrahigh mass loading. Furthermore, this 3D porous topology enabled good electron and ion transport (Figs. 16o and 16p). This LHGF/SiO material exhibited exceptional electrochemical properties with a significant discharge capacity of 35.4 mAh cm^{-2} at 8.8 mA cm^{-2}, significantly outperforming that of advanced industrial or research devices (Figs. 16q and 16r).

Anode materials based on SiO have been intensively studied as high energy density electrodes for LIBs; however, they possess relatively small ICE. Although the solid-state prelithiation of SiO with lithium hydride (LiH) has demonstrated the potential for overcoming the aforementioned problem, further advances in long-term electrochemical properties are necessary before commercialization. For example, Jeong et al. proposed a double-buffer-phase-embedded Si/$TiSi_2$/Li_2SiO_3 material generated using the phase-selective reaction of SiO with metal hydrides to enhance electrochemical properties [159]. In addition to its excellent cycling capability, the Si/$TiSi_2$/Li_2SiO_3 electrode exhibited increased thermal endurance at higher temperatures and higher rate performance, which could be linked to the recently incorporated $TiSi_2$ buffer phase (Fig. 16s).

4.2 Interface Engineering Strategy

As stated previously, alloy- and conversion-type electrode materials exhibit high irreversible capacity depletion and poor ICE as intrinsic defects. These events are caused by the strong reactivity of the Si material in contact with the electrolyte. As a result of these issues, many interfacial engineering concepts have emerged. Relevant findings from promising studies on prelithiation and artificial SEI creation are reviewed in the following sections.

4.2.1 Prelithiation Technique

A considerable preliminary irreversible capacity loss after SEI production is unavoidable for Si anodes and has a significant detrimental effect on their lifespan and properties. The addition of Li to Si materials through regulated prelithiation is an intriguing possibility. The excess Li not only offers insufficient depletion ions for SEI stability but also positively affects the ICE and boosts the working voltage [63–68]. The ability to lithiate an active material/composite anode with the most uniform lateral and in-depth distribution is vital for successful prelithiation using Li. Despite a significant amount of research on several prelithiation procedures, the precise management of the lithium quantity while maintaining a homogenous lithium distribution remains difficult. For instance, Adhitama described the thermal evaporation of Li metal as a unique prelithiation process for pure Si anodes, which enables fine control of the degree of prelithiation and homogenous Li deposition at the surface [160]. The effects of Li nucleation, mechanical cracking, and continuous phase transitions were investigated. Finally, several electrochemical procedures were used to establish a direct association between pre-SEI creation and the electrochemical properties of prelithiated Si.

The poor ICE of SiO_x anodes owing to the irreversible production of Li_2O and Li_ySiO_z during the discharging procedure restricts their application in high energy density LIBs. Li et al. presented a molten-salt-driven thermochemical prelithiation approach to control the electrochemical Si/O ratio of SiO_x, thereby increasing the ICE (Figs. 17a and 17b) [63]. Bulk SiO_x microparticles were converted into pomegranate-like prelithiated microcluster composites (M-Li-SiO_x) featuring an SiO_x core and nanosized accumulations of $Li_2Si_2O_5$, SiO_2, and Si on the exterior. To accomplish prelithiation, molten LiCl may initiate reactions and enhance diffusion through the constant extraction of oxygen components from the SiO_x particles via the study of the reaction intermediates. This level of prelithiation could be controlled by varying the exterior quantity of the $LiNH_2$ coating, and the resulting M-Li-SiO_x exhibited a significant enhancement in the ICE from 58.73% to 88.2% (Fig. 17c).

Li-containing organic molecules, such as Li-biphenyl and Li-arene complexes, have the potential to enhance the ICE when employed in chemical lithiation. Nevertheless, the production of Li-containing organic compounds required for chemical prelithiation requires metallic Li. The cautious management of exceptionally reactive Li-containing organic substances and complex activities, such as cleaning the remaining reactants and extinguishing lithiation, presents a challenge in the realistic success of the chemical lithiation procedure. Thus, exploring an Li-metal-free, safe, and scalable lithiation technique for high-capacity electrodes with high ICE is extremely desirable. Chung et al. reported an elaborate SiO-based anode exhibiting an elevated ICE (90.5%) created by Li metal-free solid-state lithiation using the LiH dehydrogenation reaction (Fig. 17d) [62]. Through the interaction of the released Li vapor with SiO, LiH was used as an Li source to create Li silicate phases in advance. The substantially greater melting temperature of LiH (692 °C) than Li metal, which results from an intense ionic connection involving Li with H in LiH, should make the

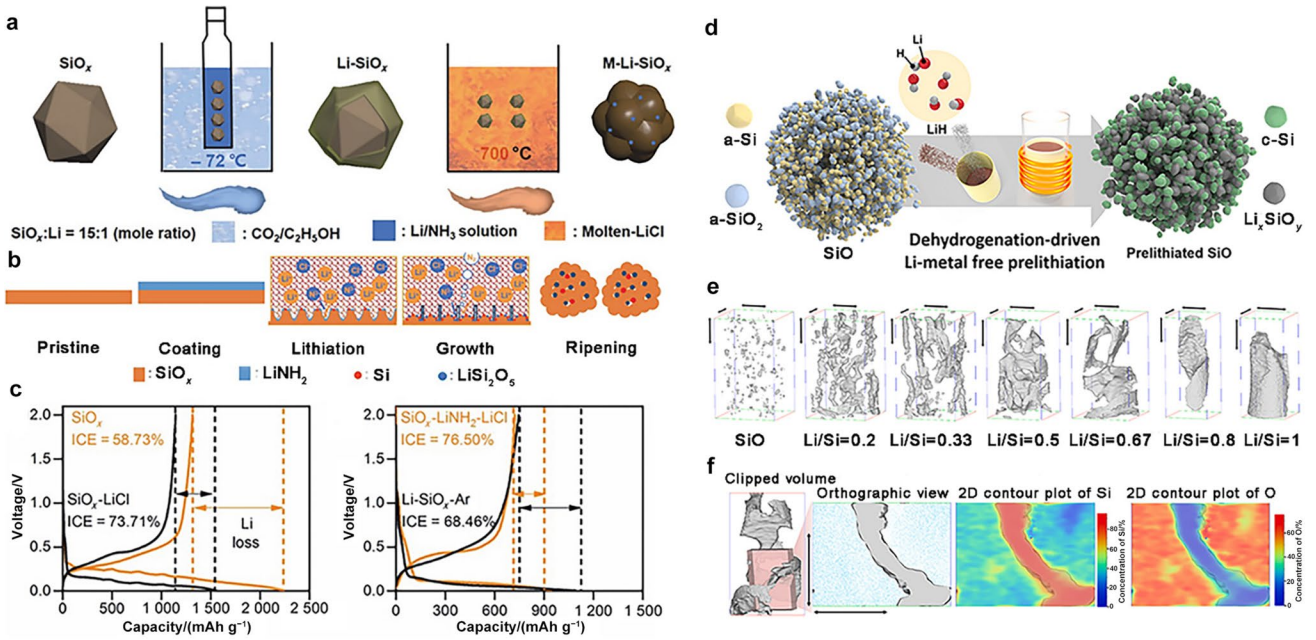

Fig. 17 **a** Scheme of the preparation of M-Li-SiO_x. **b** Schematic reaction process of M-Li-SiO_x from SiO_x. **c** Initial (dis)lithiation curves of pristine SiO_x, SiO_x-LiCl, G + SiO_x, and G + M-Li-SiO_x. Reproduced with permission from Ref. [63]. Copyright © 2021, Springer Nature. **d** Scheme of Li metal-free prelithiation induced phase change. **e** Results of the isosurface (atomic content of Si > 75%) investigation of SiO and prelithiated SiO materials. **f** Orthographic view of clipped volume, 2D contour plot of Si and O for the clipped volume, and clipped volume of prelithiated SiO (Li/Si = 0.67). Reproduced with permission from Ref. [62]. Copyright © 2021, Elsevier

prelithiation of SiO simpler and safer. Hydrogen liberated from LiH would also be extremely beneficial for establishing a reductive environment for the prelithiation of SiO. The dehydrogenation-induced lithiation of SiO using LiH led to the formation of 3D Si-Li silicate materials, which were imaged using LA-APT and STEM (Figs. 17e and 17f). They provided a capacity of 1 203 mAh g^{-1} and an ultra-high ICE of 90.5%. Full-cell studies using prelithiated SiO demonstrated a 50% increase in the energy density over pure SiO, with an outstanding lifespan beyond 800 cycles.

4.2.2 Artificial SEI Technique

With the prelithiation method, the deliberate production of an artificial SEI layer is an interesting alternative strategy for addressing early capacity loss, increasing the initial CE, and stabilizing the SEI development. As mentioned earlier, nanostructures have been demonstrated to efficiently prevent pulverization and reduce the pressure caused by significant volume growth. However, these topologies dramatically increase the surface area, which can significantly expand the scale of the SEI. Poor operating voltage, severe irreversible capacity decay, and poor cyclability have been associated with considerable SEI. Therefore, an artificial SEI layer acts as an insulating barrier, preventing materials from falling into close contact with the electrolyte and encouraging the establishment of a robust spontaneous SEI layer surrounding the Si material, thereby reducing the capacity loss [70, 124, 161–165]. Electrolyte additives, binders, surface coatings, and other materials can be used to fabricate artificial SEI layers. The desired artificial SEI layers should demonstrate outstanding chemical resistance and mechanical durability to limit the disintegration of the SEI constituents in the electrolyte and avoid the fracturing of the artificial SEI.

Ai et al. used a lithium-conducting covalent organic framework (COF) as the surface layer for SiNPs that acted as an artificial SEI for Si anodes (Figs. 18a–18d) [70]. This COF coating minimized the electrolyte breakdown, which significantly improved the CE and cycling performance. Furthermore, the enhanced Li^+ conductivity of the COF can improve the Li^+ transit dynamics. The elaborate Si anode exhibited an outstanding electrochemical performance (1 864 mAh g^{-1} after 1 000 cycles at 2 A g^{-1}). They proposed a new technique for enhancing lithium-ion diffusion kinetics by employing a COF coating as an artificial SEI, providing insights into the commercialization of Si anodes.

Cao et al. proposed adding electrolytes to develop artificial SEI layers [166]. The reasonable creation and fabrication of steady artificial interfaces for Si anodes has significant potential for protecting materials from inherent volume variations and mitigating adverse effects, both of which are required for high-capacity Si-based anodes. When the electrodes were dried at an elevated temperature, a multifunctional SEI precursor consisting of a

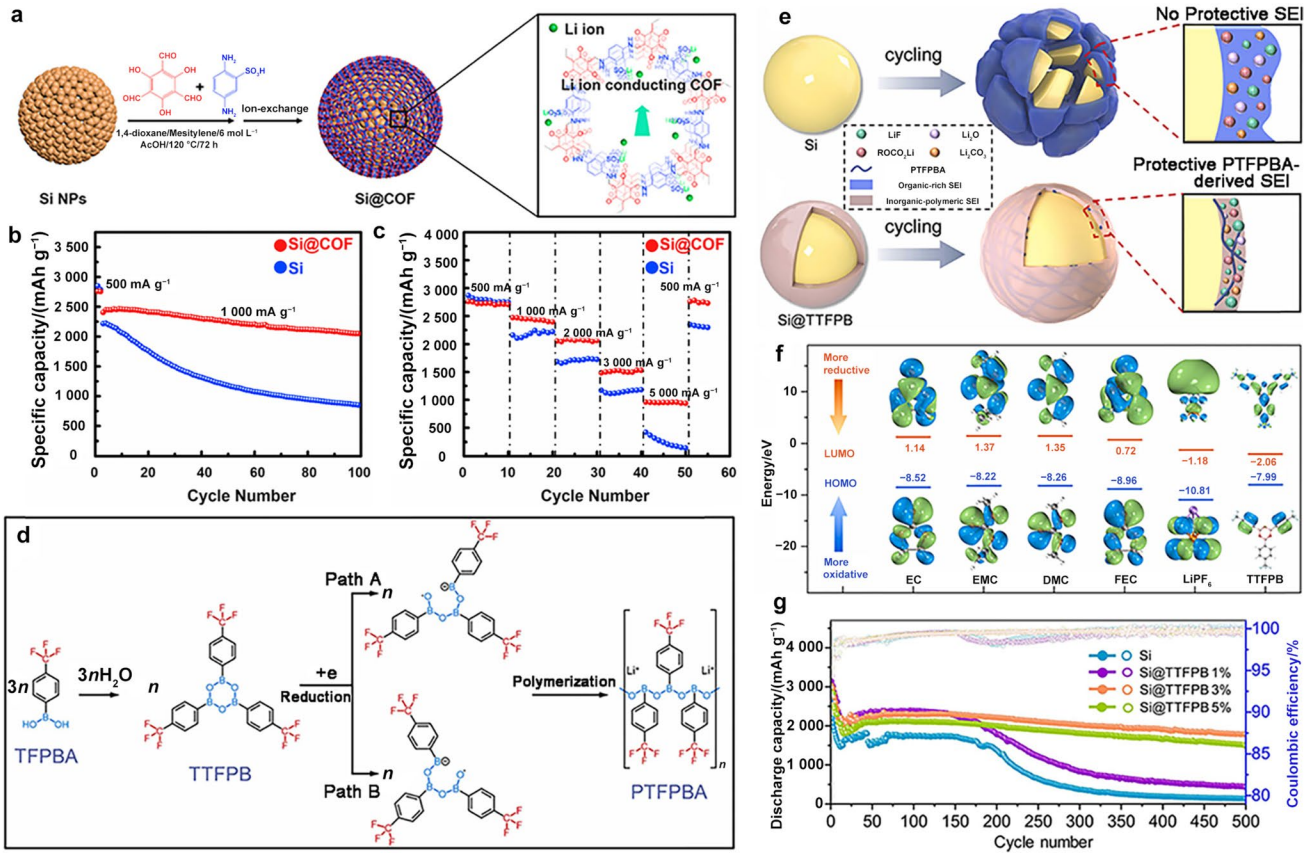

Fig. 18 **a** Synthesis of Si@COF NPs. **b** Cycling properties, **c** rate behavior of pristine Si and Si@COF at 1.0 A g^{-1}. Reproduced with permission from Ref. [70]. Copyright © 2020, Elsevier. **d** Potential pathways for TTFPB's electrochemical reductive breakdown. **e** Illustrative diagrams of defense process using implanted TTFPB nanolayer. **f** Estimated HOMO and LUMO energy for various molecules. **g** Cycling properties of pristine Si and Si@TTFPB at 0.2 C. Reproduced with permission from Ref. [166]. Copyright © 2022, Elsevier

4-trifluoromethylphenylboronic acid (TFPBA) nanolayer was designed and rapidly polymerized to create 2,4,6-trifluoromethylphenyl) boroxine (TTFPB) on the exterior. After one-electron reduction, the B–O bonds of the TTFPB molecule ruptured, leading to the creation of revolutionary molecules and the beginning of random polymerization to produce poly-4-trifluoromethylphenylboronic acid (PTFPBA) with repeated B–O chains (Figs. 18e and 18f). Polymerized nanolayers not only exhibit the desired artificial SEI because of their high resilience and flexibility in tolerating volume changes, but also significantly increase the electrolyte absorbency of the electrode, providing faster Li^+ kinetics. This steady scheme produced by PTFPBA enabled the majority retention of $LiPF_6$ molecules with electron-deficient boron (B) species, which produced a constant and thick SEI rich in benzene rings and inorganic compounds (Fig. 18g). Consequently, the acquired Si@TTFPB anode exhibited improved electrochemical performance (1 778.7 mAh g^{-1} after 500 cycles at 0.2 C) (Fig. 18h).

4.3 Novel Binder Design

Binders are necessary components in the manufacturing of electrodes, serving to glue the active ingredient, conductive carbon, and current collector together while staying intact [167–178]. Despite their small fraction (5%), they are critical for Li ions. The long-term cycling stability of a battery is crucial. Conventional CMC/SBR or PVDF binders can satisfy the application requirements for graphite anodes because of the minor volume expansion (10%) throughout the (de)lithiation procedure. However, silicon-based anodes exhibit significant volume variations (up to 300%), which places higher demands on the thorough characteristics of the binder. The high-performance polymer binder efficiently suppresses volume expansion, maintains conductivity and integrity during the discharging/charging process, and considerably improves the cycling stability [179–188]. The following subdivisions discuss advances in innovative conductive, elastic, and self-healing binders that have the potential to improve the durability of Si-based anodes (Fig. 19 and Table 2).

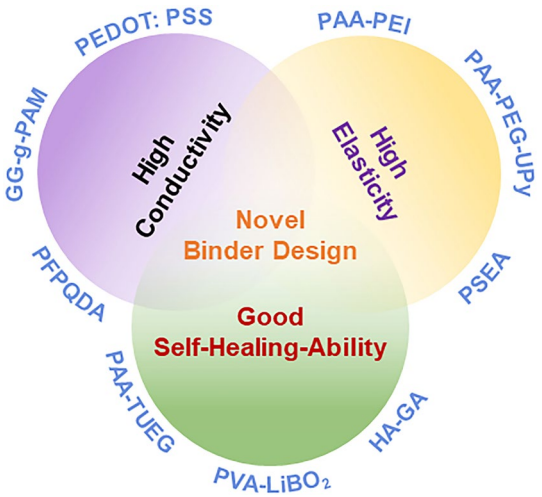

Fig. 19 Schematic of multiple binders for Si-based electrodes

4.3.1 Conductive Binder

The shielding qualities of traditional binders make it difficult for the cells to undergo electrochemical reactions. Several conductive binders have been proposed to improve the performance. Conduit-conducting additives can simultaneously function as binders and conductors to shorten the ionic/electronic diffusion pathways and boost the energy density and surface reactivity [189, 190]. Based on their innate characteristics, conductive binders can be classified as electronic and ionic conductors. The electrical integrity of the entire electrode may be successfully improved, and Si detachment from the substrate during volume variations can be prevented using a binder that has outstanding conductivity and robust contact with the electrode materials. To strengthen their bonds with Si materials, conductive binders have certain conductive compounds as their structural foundation, which are then adorned with additional nonpolar or polar groups.

Binders are required to reduce mechanical strain and increase the cycle durability of Si anodes. Li et al. developed a strain-distributed binder with high electrical conductivity (GG-g-PAM) by laminating polyacrylamide (PAM) over an ion-conductive guar gum (GG) framework [191]. The strain concentration on the attached PAM chain promoted tension dispersion in the GG-g-PAM binder, leading to steady electrode-electrolyte contact during (de)lithiation. Peak-force AFM and finite element simulations supported the potential of the GG-g-PAM binder to dissipate stress (Fig. 20a). The remarkable cyclability of the Si anode-based Ah-level pouch cells firmly established GG-g-PAM as a suitable binder for real-world commercialization.

A conductive binder can address this problem by preserving continuous electron pathways during the Si pulverization. Kim et al. synthesized poly(3,4 ethylenedioxythiophene):poly(styrene sulfonate) (PEDOT:PSS) and PVA as Si-based electrode materials, which generated a multilayered architecture because of the various chain diameters of polyethylene glycol (PEG) and polyethylene oxide (PEO) [192]. When PEO or PEG was used, the electrical conductivity (40%) and stretchability (60%) increased because of the extensively dispersed hydrogen linkages and connections. A silver nanowire (AgNW) architecture paired with a polymer binder provides an efficient 3D electrical channel, a sufficient empty area to accommodate volume changes, and sticky contact with the Cu collector. After 100 cycles, this manufactured Si electrode material had a supreme cycling property of 1 066 mAh g^{-1} at 0.8 A g^{-1}.

4.3.2 Elastic Binder

Although conductive binders enable quick electronic/ionic diffusion pathways, their limited mechanical characteristics

Table 2 Summary of various novel binders and corresponding electrochemical performance of Si-based electrodes reported previously

Electrode material	Binder	Cutoff voltage	[Capacity/(mAh g^{-1})]/[current density/(mA g^{-1})]/cycle number/capacity retention	Ref.
PNAGA-Si	Poly(*N*-acryloyl glycinamide)	0.01–1.2	2 931/0.42/100/84.0%	[152]
Si@CS-g-GA	Chitosan-grafted gallic acid	0.01–1.5	1 868/0.5/350/67.0%	[156]
SiO_x	CMC-Na	0.01–1.0	571.8/0.4/500/53.2%	[157]
Si/C	CMC/EDTA-Ca^{2+}	0.01–1.5	602.0/1.0/380/80.7%	[158]
SiO_x/PGA-ECH	γ-Polyglutamic acid cross-linked by epichlorohydrin	0.01–3.0	900.5/0.5/500/73.2%	[159]
Si-PAA-β-CD_p	Polyacrylic acid and polymerized β-cyclodextrin	0.01–1.5	2 326/0.2/100/64.6%	[160]
Si	An endotenon sheath-inspired double-network binder	0.01–1.5	1 115/4.2/300/56.8%	[164]
Si-Gr	Pyrene-conjugated poly(acrylic acid) and γ-cyclodextrin polymer	0.01–1.0	328.6/0.5/200/80.2%	[166]
Si/C	Alginate-grafted polyacrylamide and aniline tetramer	0.01–3.0	1 623.7/0.5/300/79.2%	[167]
Si@CGN	Polysaccharide lambda carrageenan	0.01–1.5	770.5/0.5/500/78.2%	[170]

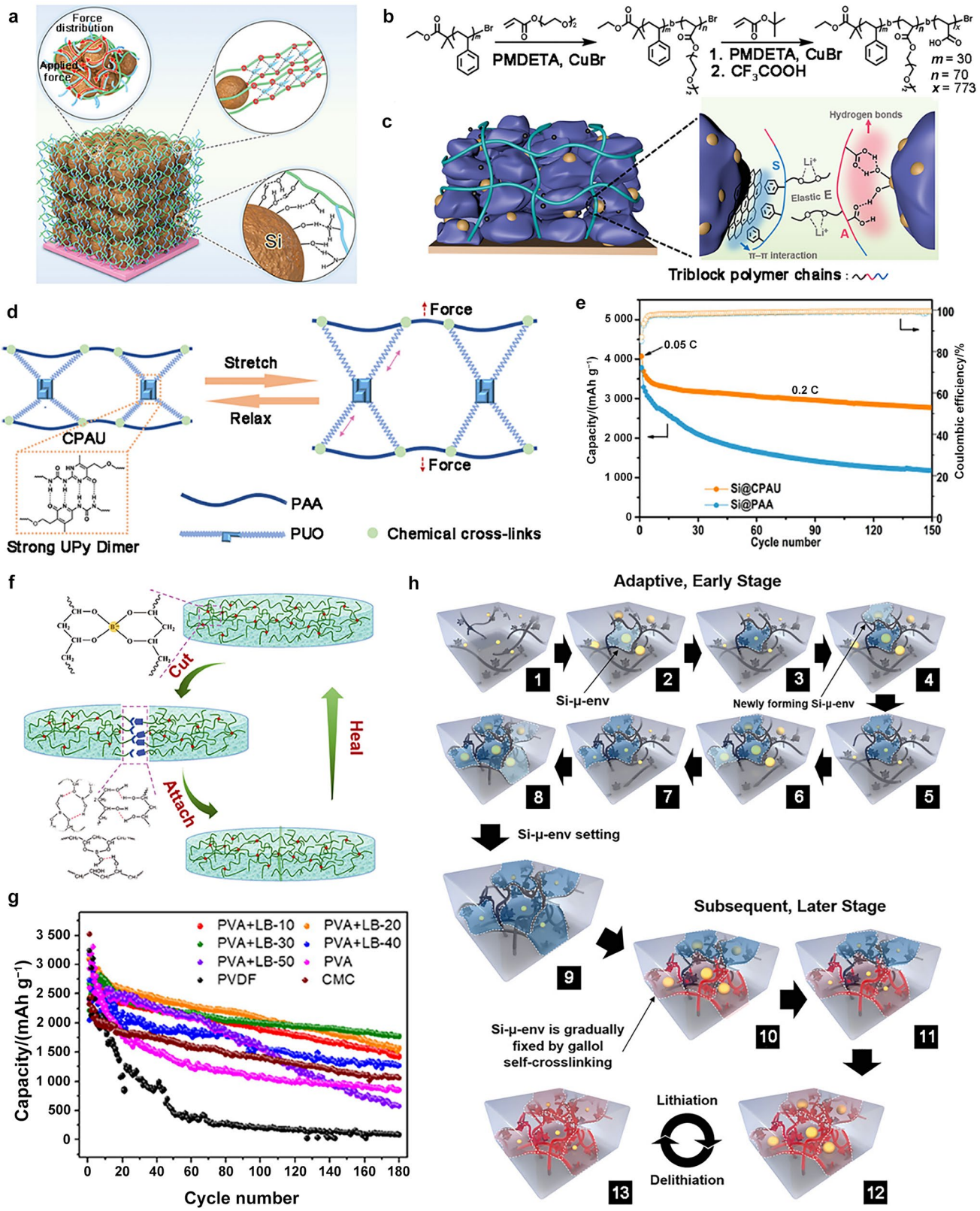

may result in mechanical fractures and disintegration of the active substance from the Cu collector. Elastic binders have attracted the interest of researchers because of their capacity to withstand significant mechanical stresses driven by volume variations in Si anodes. The interfacial diffusion dynamics improved, electrode fracturing was effectively

◂**Fig. 20** **a** Potential GG-g-PAM binder function in Si anode. Reproduced with permission from Ref. [191]. Copyright © 2022, Wiley-VCH. **b** Synthetic scheme of triblock polymer PSEA. **c** Scheme of π···π interaction between carbon and phenyl groups as well as hydrogen bonds between Si particles and carboxyl group of PSEA binder. Reproduced with permission from Ref. [194]. Copyright © 2022, Wiley-VCH. **d** Scheme of elastic properties of CPAU and **e** cycling performance of electrode materials. Reproduced with permission from Ref. [195]. Copyright © 2021, American Chemical Society. **f** Scheme of self-healing procedure and **g** cycling performance of electrode materials. Reproduced with permission from Ref. [196]. Copyright © 2022, Elsevier. **h** Comprehensive scheme of a gallol-conjugated binder's molecular mobility in Si-microenvironments (Si-μ-env, the blue areas). Reproduced with permission from Ref. [197]. Copyright © 2021, Wiley-VCH

avoided, and SEI growth was stabilized by the addition of Si anodes with elevated elastic modulus polymer binders. Binders possess elastic qualities owing to their inherent intermolecular interactions, particularly hydrogen bonds, which allow them and active materials to repair damage and return to their original state. To offer persistent contact even after volume fluctuations, it is necessary to strengthen the connection between the elastic binders and Si anodes by hydrogen or chemical bonding.

Although adhesive polymeric binders, including PAA, ameliorate these severe volumetric variations, the cycling capabilities of the synthesized Si anodes do not satisfy the criteria for potential implementation. Shi et al. described a unique polymer binder that included PAA, a chemical switch (NH_3), and a cross-linker (polyethyleneimine) [193]. In this slurry, the interaction between PAA and PEI stopped and may have later returned during electrode drying. After 150 cycles, the Si anode manufactured with the PAA-PEI-c binder exhibited an outstanding capacity retention of 67% compared to the PAA anodes in half-cells. In addition, the PAA-PEI-c binder outperformed PAA in the full cells. Furthermore, compared to the standard electrode lamination technique, this approach requires no additional processes, indicating its significant potential for immediate implementation in large-scale manufacturing. Hu et al. reported the development of an interface-adaptive triblock polymer binder that interacts with Si and graphite fragments to boost component inclinations and binder dissemination through the supramolecular engagement of the pi-pi arrangement and hydrogen bonding [194]. The Si/C anode maintained a high cycling stability (82.1%) after 400 cycles. This elaborate binder method lays a foundation for improving the Si/C anodes. Liu et al. designed a polymer binder with an exceptionally adaptable and stretchable framework capable of accommodating Si volume change [195]. During electrode production, PAA is cross-linked in situ with urethane-dissolved polymeric monomers consisting of PEG chains and 2-ureido-4-pyrimidinone (UPy) units. By establishing hydrogen bonds involving the exterior hydroxyl chains, PAA can firmly bind to the Si particles within this binder network. The PEG chains enabled the polymer matrix to bend more easily, whereas the UPy functionalities offered sufficient durability to the polymer matrix by creating reversible and resilient quadruple H-bonding cross-linkers (Figs. 20d and 20e). The binder not only accommodates the Si volume fluctuations but also provides adequate compressive assistance to efficiently retain the functionality of the Si anode, thereby enhancing the cycle stability.

4.3.3 Good Self-Healing-Ability Binder

Self-healing is the capacity of a substance to mend itself after being destroyed and was first identified as a simple method for fixing mechanical cracks in biological structures. Natural self-healing is currently implemented in Si anodes and is critical for solving similar difficulties [167, 185]. For example, by dissolving a suitable quantity of LB in longitudinally polymerized PVA, Zhao et al. created a special PVA + $LiBO_2$ (LB) material that functioned as a self-healing binder for outstanding-durability electrode materials [196]. The spontaneous cross-linking of PVA and boric acid produces a 3D network within the PVA + LB binder. The electrochemical properties of the Si anodes utilizing PVA + LB as the binder were significantly enhanced compared to those of PVDF, CMC, and PVA. It was selected because of its improved adaptability and consistency, self-healing features, 3D network architecture, and suitable content (Figs. 20f and 20g). According to the results of the electrochemical experiments, the cycling stabilities of the Si (1 773.0 mAh g^{-1} at 400 mA g^{-1}) and Si/C (861.7 mAh g^{-1} at 1 A g^{-1}) electrode materials were enhanced. The capacity of future Si anodes can be maintained using the present inorganic cross-linked supramolecular binder.

To address the issue, Lee et al. recently announced their idea of an "adaptive binder" [197]. When cycling caused gradual changes in the microenvironment around the Si particles, the binders exhibited flexibility. When micro-Si progressively emerges during the early battery cycles, the long flexible binder chains move and are reoriented. Reversible hydrogen bonds are the dominant type of chemical interactions between the polymeric binders at this stage. Chemical associations demonstrate reversible-to-irreversible changes by creating covalent bonds between the binder polymers, because micro-Si is firmly formed over numerous cycles. Hyaluronic acid is an adaptable binder polymer that has not been studied for Si anodes (Fig. 20h). Gallol (1,2,3-trihydroxybenzene), an aromatic component of plants, was attached to HA-GA for robust adhesion to the exterior of Si particulates. After 600 cycles, the HA-GA binder continued to hold a charge capacity approximately 3.3 times greater (1 153 mAh g^{-1}) than that of the nonconjugated HA binder

(347 mAh g^{-1}), suggesting that flexible qualities are vital when constructing Si anode binders, even at 1 C.

4.4 Innovative Electrolyte Design

The creation of improved electrolytes with the development of multifunctional binders is essential for enhancing cycling stability. The mechanical performance of Si anodes during cycling can be enhanced using an appropriate electrode composition and binders. The significant volume change of the Si anode during lithiation caused the SEI coating to continuously fracture and rebuild on its exterior. Increasing the thickness of the SEI results in an increase in the interface impedance and a reduction in the battery capacity. Consequently, the components, architecture, and external properties of the SEI have a direct impact on the electrochemical behavior. A thick and steady SEI layer is important for ensuring electrochemical performance. Thus, modifying the electrolyte by adjusting its composition and amount is critical for enhancing the electrochemical properties of Si-based anodes (Table 3) [198–205].

4.4.1 FEC

Among the most effective and practical methods for preventing substantial volume variations and inadequate ICE caused by unconstrained electrolyte breakdown in high energy density anodes, such as Li metal and Si anodes, is the incorporation of a small quantity of extraneous biodiversity, which is referred to as an efficient ingredient. One of the most efficient components for boosting the electrochemical properties of Si anodes is FEC, whose rapid defluorination and subsequent polymerization gives the SEI greater versatility as well as an elevated LiF concentration [206–213]. The inequitable buildup of the SEI on the Si exterior is a significant impediment to the cycle stability. According to the molecular makeup, ideal reductive and oxidative electrolyte additions should possess lower LUMO and higher HOMO norms, respectively. There has been considerable interest in the addition of certain functional electrolytes, including CO_2, ionic additives, silane-type compounds, and nitrogen-containing additives. Recently, various important and effective efforts toward the addition of electrolytes for SEI remediation have been emphasized. Haridas et al. studied the significance of FEC and TTMSP as electrolyte additives in the design of high-capacity Si-NMC-based FCs [213]. The mSi/pPAN and NMC532 anodes with multiple TTMSP and FEC ratios demonstrated that increasing the TTMSP content had a favorable impact on achieving steady electrochemical properties for the NMC532 cathode, most likely by decreasing the HF-mediated transition metal loss. SEM patterns following cycling, charge-discharge experiments, and resistance evaluation of the mSi/pPAN anode indicated a nonuniform SEI and decreased reversible capacity. According to the experimental data, the passivation coating generated by TTMSP on the mSi/pPAN anode may not be uniform in the absence of FEC. This demonstrates that the TTMSP additive generates a robust and conductive surface coating, which preserves the cathode stability and reduces the cell IR by preventing transition metal loss. Furthermore, the presence of FEC in the electrolyte facilitates the formation of a high energy density mSi/pPAN anode. The long cycle life of the mSi/pPAN-NMC532 FC confirmed the synergistic effect of TTMSP and FEC. This highlights the necessity of selecting multi-electrolyte additives in appropriate proportions to passivate both the anode

Table 3 Summary of various advanced electrolyte additives and corresponding electrochemical performance of Si-based electrodes reported previously

Electrode material	Electrolyte additives/usage amount	Cutoff voltage	[Capacity/(mAh g^{-1})]/[current density/(mA g^{-1})]/cycle number/capacity retention	Ref.
Si@HEDP	1-Hydroxyethylidene-1,1-diphosphonic acid/7% by weight	0.01–1.0	1 831/0.84/500/82.7%	[183]
Si-APTES-5%	(3-Aminopropyl)triethoxysilane/5% by weight	0.01–1.0	2 132/0.2/50/83.2%	[184]
Si@C/$LiNi_{0.5}Mn_{1.5}O_4$	Lithium difluorophosphate and 1,3,6-hexanetrinitrile/(1% + 1%) by weight	0.005–2.0	123/0.2/150/91.6%	[189]
Si@graphene	2-Isocyanatoethylmethacrylate and fluoroethylene carbonate/(1% + 9%) by volume	0.01–1.5	1 373/1.0/500/99.0%	[192]
Si-LEDC	$SiCl_4$ additive/3% by weight	0.01–1.5	1 617/0.2/100/51.5%	[193]
VC-milled Si	Vinylene carbonate/2% by weight	0.01–3.0	1 235/0.2/50/49.2%	[195]
Si-S@pPAN	Lithium difluorophosphate and *N*,*N*-dimethyltrifluoroacetamide/(2% + 2%) by weight	0.01–1.0	1 400/2.0/1 000/92.1%	[196]
Si/C	Trifluoropropylene carbonate/10% by weight	0.01–1.5	1 545/0.2/200/52.8%	[198]
NMC-111‖Si full cells	Lactic acid *o*-carboxyanhydride/2% by weight	3.0–4.3	136.6/0.2/100/51.6%	[199]

and cathode surfaces in mSi/pPAN-NMC532 FCs for high capacity and extended cycle performance.

4.4.2 Vinylene Carbonate

Another distinguished electrolyte, vinylene carbonate (VC), is currently marketed to boost the cycling properties. VC was initially developed to increase the capability of graphite anodes; however, it can also be used to regulate SEI film formation in Si-based electrodes. Owing to its flexibility, VC was more effective than FEC in increasing the longevity and efficiency of both half and whole cells. Salah et al. investigated the impact of adding 5% VC to a conventional electrolyte on the performance of physically vapor-produced Si thin films [203]. Charge/discharge cycling, cyclic voltammetry (CV), and electrochemical impedance spectroscopy (EIS) were employed to study the variations in the battery cycling parameters (i.e., cutoff voltages), revealing that these changes had a significant impact on the cycling performance of the anodes. Each operation (electrolyte additive and battery cycling regimen) was studied to determine its influence on the initial discharge capacity, irreversible capacity, and capacity retention. The Si film with optimal deposition conditions, electrolyte additives, and battery testing techniques demonstrated a discharge capacity of 1 740 mAh g^{-1} and capacity retention of 92% at C/2 after 1 000 cycles.

5 Summary and Outlook

Si-based materials have great potential as anodes for LIBs because of their outstanding energy densities, low cost, and adequate working voltages. Although they exhibit numerous valuable properties, two major obstacles hinder their broad application: (i) large lithiation-driven volume changes and (ii) unsteady SEI development. In this paper, we addressed the key problems and cutting-edge breakthroughs in increasing the stability of Si-based electrodes. First, the failure process was thoroughly examined. The second section discussed the sophisticated in situ/operando characterization methods that are currently used to evaluate electrochemical reactions, structural development, and degradation processes. To address these issues, we discussed the concepts of the structural design, surface/interface engineering, and new binders/electrolytes. In addition, we highlighted several essential points for further research and advancement.

1. The failure mechanisms of Si-based full batteries, and not just Si-based anodes, should be thoroughly analyzed to provide effective and targeted solutions for enhancing the cycling stability. The qualitative and quantitative evaluation of the in situ responses involving Li with Si throughout the (dis)charge procedure is crucial. Despite the fact that in situ evaluations such as SEM, TEM, and XRD may be helpful for assessing multiple chemical reactions on the exterior of Si materials, sophisticated analytical techniques (such as in situ FTIR, cryo-EM, AFM, and NMR) and computational approaches should be constructed and combined to clarify the connections between the capacity and structure at the atomic or molecular level, which will provide useful knowledge and advice regarding subsequent material architecture.
2. Understanding the structure-property connection of the interphase is a crucial aspect toward the forthcoming architecture of SEI. A practical approach for the reasonable refinement and customization of the desired chemistry and characteristics of the multilayer interphase is the prudent construction of an artificial SEI. Predictive computer modeling may be used to enhance artificial SEI, especially when paired with information and the accurate evaluation of pertinent electrode surface-coating processes. A uniform thin insulating layer with an even thickness and distribution may be applied at the atomic level to electrode surfaces using techniques such as atomic layer deposition and molecular layer deposition.
3. To inhibit volume variations and stabilize SEI production, large amounts of innovative elastic/conductive binders and electrolyte additives have been added to Si anodes. Elastic binders were demonstrated to successfully relieve strain, although only a few binders have been studied, such as styrene-butadiene rubber and PAA, which are commercially accessible. Therefore, additional research on effective binders and electrolyte additives that preserve intact structures and encourage the creation of steady SEI should be conducted. Moreover, freestanding membranes and binder-free electrodes without current collectors have been demonstrated to increase the areal capacity and energy density, while also showing potential in flexible electronic devices.
4. These techniques aim to reduce the oxides on the surface of Si anodes. Si oxides undoubtedly cause severe irreversible side reactions during the initial discharge process, resulting in noticeably lower ICE values. This is somewhat debatable, although some studies have shown that the presence of partially oxidized Si is advantageous for extending the lifetime. To manufacture Si anodes with an elevated ICE and outstanding cycle stability, novel findings regarding the architecture and controlled fabrication of Si with atomic dispersion in graphitic carbon and/or Si with protective substances on the exterior should be highlighted.
5. Safety is an essential characteristic for assessing the performance of batteries. Unavoidable volume changes, erratic SEI formation, and electrolyte degradation in LIBs can result in significant Li-dendrite production, leading to short circuits and cell explosions. Solid-state

batteries with solid electrolytes are an optimal solution to this challenge because they can be produced using various methods to power portable and wearable devices. Currently, solid-state batteries have insufficient electrical and ionic conductivities for mass manufacturing. To address the enormous energy demand of EVs, HEVs, and portable devices, this innovation should be rapidly enhanced toward practical use.

6. Polarized electrodes, electrolytes, and interphases have interfacial processes and related chemistry that are typically considered separate from one another. Nevertheless, mounting data revealed cross-talk between the two. This is because of the frequency at which the species created on one electrode appear in the opposite compartment, often causing unintended negative effects. Owing to the severe (electro)chemical conditions present in both electrode compartments of Si-based||Ni/Li-rich batteries, this problem has become critical (e.g., an unsteady SEI film on the anode and cathode that actively releases oxygen). The repeated cycling of low-working-voltage (e.g., 0.2 V vs. Li/Li^+) (de)lithiation procedures promotes the preset voltage of the cathode, which lowers the cycling efficiency, encourages capacity decline, and increases impedance. Consequently, the development of high-energy Si-based electrode materials requires a comprehensive analysis of the interactions among the electrodes, electrolytes, and interphases, as well as their intricate chemistry.
7. Machine learning (ML) approaches, with other research instruments, are valuable for sophisticated battery data evaluation. Refined ML methods, such as extrapolation, with different algorithms, may forecast the cycle life of a battery according to data such as the capacity, voltage, and current rate. Furthermore, ML-based techniques can assist in the prediction of multiple battery material features, as well as the elucidation of connections between material details (e.g., the thickness of the outermost coating of an Si anode) and battery capacity, whether certain features have a greater influence than others, and even some deeper connections between them.
8. Several forms of mechanical deterioration in batteries have been discovered using recently established research methods; however, it is difficult to measure the level of breakdown during battery operation. One method for efficiently quantifying corrosion in batteries is to use cutting-edge data-driven modeling to explicitly associate the extent of mechanical damage with cycle variables, such as the charging rate and cutoff window. Based on the insights gained from data-driven simulations, it is possible to further cultivate theoretical frameworks to forecast the evolution of mechanical damage during battery operation, similar to the commonly utilized Paris law, to characterize fatigue crack growth under cyclic mechanical loads. These basic models have the potential for application in the battery sector.
9. The development of cycling procedures that enable quick and/or deep charging while preventing mechanical battery degradation is appealing from an industrial perspective. Utilizing the most recent data-driven methodology to enhance charging methods is one such technique. This method can overcome the requirement for explicit comprehension of the intricate chemomechanical relationships in batteries that control their performance. However, the collection of datasets, such as those of batteries that have intentionally undergone varying degrees of mechanical degradation caused by various cycling protocols, necessitates the ongoing development of scientific methods that can produce data for research at an unprecedented rate.

This review presents a practical method for constructing high-energy Si-based LIBs with low cost, high security, and superior cycling stability, which can guide further studies and construction of alloy-based materials and batteries.

Acknowledgements This study was financially supported by the National Natural Science Foundation of China (Grant Nos. U22A20420, 22078029, 22208029, and 52203292), Postgraduate Research & Practice Innovation Program of Jiangsu Province (Grant No. KYCX23_3027) and the "333 high-level talent training project" young and middle-aged leading talent project of Jiangsu Province. The authors thank the Jiangsu Development and Reform Commission for their support.

Declarations

Conflict of interest The authors declare no competing financial interest.

References

1. Fan, E.S., Li, L., Wang, Z.P., et al.: Sustainable recycling technology for Li-ion batteries and beyond: challenges and future prospects. Chem. Rev. **120**, 7020–7063 (2020). https://doi.org/10.1021/acs.chemrev.9b00535
2. Guo, J.P., Dong, D.Q., Wang, J., et al.: Silicon-based lithium ion battery systems: state-of-the-art from half and full cell viewpoint. Adv. Funct. Mater. **31**, 2102546 (2021). https://doi.org/10.1002/adfm.202102546
3. Yin, Y.X., Wan, L.J., Guo, Y.G.: Silicon-based nanomaterials for lithium-ion batteries. Chin. Sci. Bull. **57**, 4104–4110 (2012). https://doi.org/10.1007/s11434-012-5017-2
4. Zhu, G.J., Chao, D.L., Xu, W.L., et al.: Microscale silicon-based anodes: fundamental understanding and industrial prospects for practical high-energy lithium-ion batteries. ACS Nano **15**, 15567–15593 (2021). https://doi.org/10.1021/acsnano.1c05898
5. Eshetu, G.G., Zhang, H., Judez, X., et al.: Production of high-energy Li-ion batteries comprising silicon-containing anodes and insertion-type cathodes. Nat. Commun. **12**, 5459 (2021). https://doi.org/10.1038/s41467-021-25334-8

6. Etacheri, V., Marom, R., Elazari, R., et al.: Challenges in the development of advanced Li-ion batteries: a review. Energy Environ. Sci. **4**, 3243 (2011). https://doi.org/10.1039/c1ee01598b
7. Chae, S., Ko, M., Kim, K., et al.: Confronting issues of the practical implementation of Si anode in high-energy lithium-ion batteries. Joule **1**, 47–60 (2017). https://doi.org/10.1016/j.joule.2017.07.006
8. Zhao, L., Zhang, D.F., Huang, Y.F., et al.: Constructing a reinforced and gradient solid electrolyte interphase on Si nanoparticles by in-situ thiol-ene click reaction for long cycling lithium-ion batteries. Small **17**, e2102316 (2021). https://doi.org/10.1002/smll.202102316
9. Yuda, A.P., Koraag, P.Y.E., Iskandar, F., et al.: Advances of the top-down synthesis approach for high-performance silicon anodes in Li-ion batteries. J. Mater. Chem. A **9**, 18906–18926 (2021). https://doi.org/10.1039/d1ta02711e
10. Wei, T.T., Peng, P.P., Ji, Y.R., et al.: Rational construction and decoration of $Li_5Cr_7Ti_6O_{25}$@C nanofibers as stable lithium storage materials. J. Energy Chem. **71**, 400–410 (2022). https://doi.org/10.1016/j.jechem.2022.04.017
11. Yi, T.F., Mei, J., Peng, P.P., et al.: Facile synthesis of polypyrrole-modified $Li_5Cr_7Ti_6O_{25}$ with improved rate performance as negative electrode material for Li-ion batteries. Compos. Part B Eng. **167**, 566–572 (2019). https://doi.org/10.1016/j.compositesb.2019.03.032
12. Yi, T.F., Shi, L.N., Han, X., et al.: Approaching high-performance lithium storage materials by constructing hierarchical $CoNiO_2$@CeO_2 nanosheets. Energy Environ. Mater. **4**, 586–595 (2021). https://doi.org/10.1002/eem2.12140
13. Zheng, G.R., Xiang, Y.X., Xu, L.F., et al.: Controlling surface oxides in Si/C nanocomposite anodes for high-performance Li-ion batteries. Adv. Energy Mater. **8**, 1801718 (2018). https://doi.org/10.1002/aenm.201801718
14. Lu, W.J., Guo, X.T., Luo, Y.Q., et al.: Core-shell materials for advanced batteries. Chem. Eng. J. **355**, 208–237 (2019). https://doi.org/10.1016/j.cej.2018.08.132
15. Shen, C.F., Fang, X., Ge, M.Y., et al.: Hierarchical carbon-coated ball-milled silicon: synthesis and applications in free-standing electrodes and high-voltage full lithium-ion batteries. ACS Nano **12**, 6280–6291 (2018). https://doi.org/10.1021/acsnano.8b03312
16. Guo, K., Kumar, R., Xiao, X.C., et al.: Failure progression in the solid electrolyte interphase (SEI) on silicon electrodes. Nano Energy **68**, 104257 (2020). https://doi.org/10.1016/j.nanoen.2019.104257
17. Gu, L.H., Han, J.J., Chen, M.F., et al.: Enabling robust structural and interfacial stability of micron-Si anode toward high-performance liquid and solid-state lithium-ion batteries. Energy Storage Mater. **52**, 547–561 (2022). https://doi.org/10.1016/j.ensm.2022.08.028
18. Gao, X., Lu, W.Q., Xu, J.: Insights into the Li diffusion mechanism in Si/C composite anodes for lithium-ion batteries. ACS Appl. Mater. Interfaces **13**, 21362–21370 (2021). https://doi.org/10.1021/acsami.1c03366
19. Ren, Y.R., Li, M.Q.: Facile synthesis of SiO_x@C composite nanorods as anodes for lithium ion batteries with excellent electrochemical performance. J. Power Sources **306**, 459–466 (2016). https://doi.org/10.1016/j.jpowsour.2015.12.064
20. Kohler, T., Hadjixenophontos, E., Joshi, Y., et al.: Reversible oxide formation during cycling of Si anodes. Nano Energy **84**, 105886 (2021). https://doi.org/10.1016/j.nanoen.2021.105886
21. Sun, C.L., Wang, Y.J., Gu, H., et al.: Interfacial coupled design of epitaxial graphene@SiC Schottky junction with built-in electric field for high-performance anodes of lithium ion batteries. Nano Energy **77**, 105092 (2020). https://doi.org/10.1016/j.nanoen.2020.105092
22. Zhang, Y., Wang, Z.Y., Hu, K., et al.: Anchoring silicon on the basal plane of graphite via a three-phase heterostructure for highly reversible lithium storage. Energy Storage Mater. **34**, 311–319 (2021). https://doi.org/10.1016/j.ensm.2020.10.002
23. Wu, H., Cui, Y.: Designing nanostructured Si anodes for high energy lithium ion batteries. Nano Today **7**, 414–429 (2012). https://doi.org/10.1016/j.nantod.2012.08.004
24. Yan, Z.L., Liu, Y.J., Hatchard, T.D., et al.: Quantitative measurement of solid electrolyte interphase growth on Si-based anode materials. J. Power Sources **530**, 231281 (2022). https://doi.org/10.1016/j.jpowsour.2022.231281
25. Li, X.Z., Zhang, N., Wu, Y.R., et al.: Interconnected $Bi_5Nb_3O_{15}$@CNTs network as high-performance anode materials of Li-ion battery. Rare Met. **41**, 3401–3411 (2022). https://doi.org/10.1007/s12598-022-02049-3
26. Wu, H., Zheng, G.Y., Liu, N., et al.: Engineering empty space between Si nanoparticles for lithium-ion battery anodes. Nano Lett. **12**, 904–909 (2012). https://doi.org/10.1021/nl203967r
27. Ren, W.F., Li, J.T., Zhang, S.J., et al.: Fabrication of multi-shell coated silicon nanoparticles via in-situ electroless deposition as high performance anodes for lithium ion batteries. J. Energy Chem. **48**, 160–168 (2020). https://doi.org/10.1016/j.jechem.2020.01.001
28. Ge, M.Z., Tang, Y.X., Malyi, O.I., et al.: Mechanically reinforced localized structure design to stabilize solid-electrolyte interface of the composited electrode of Si nanoparticles and TiO_2 nanotubes. Small **16**, e2002094 (2020). https://doi.org/10.1002/smll.202002094
29. Wu, Y.J., Chen, Y., Huang, C.L., et al.: Small highly mesoporous silicon nanoparticles for high performance lithium ion based energy storage. Chem. Eng. J. **400**, 125958 (2020). https://doi.org/10.1016/j.cej.2020.125958
30. Song, M.S., Chang, G., Jung, D.W., et al.: Strategy for boosting Li-ion current in silicon nanoparticles. ACS Energy Lett. **3**, 2252–2258 (2018). https://doi.org/10.1021/acsenergylett.8b01114
31. Hu, L., Luo, B., Wu, C.H., et al.: Yolk-shell Si/C composites with multiple Si nanoparticles encapsulated into double carbon shells as lithium-ion battery anodes. J. Energy Chem. **32**, 124–130 (2019). https://doi.org/10.1016/j.jechem.2018.07.008
32. Wilson, A.M., Way, B.M., Dahn, J.R., et al.: Nanodispersed silicon in pregraphitic carbons. J. Appl. Phys. **77**, 2363–2369 (1995). https://doi.org/10.1063/1.358759
33. Tian, H., Tian, H.J., Yang, W., et al.: Stable hollow-structured silicon suboxide-based anodes toward high-performance lithium-ion batteries. Adv. Funct. Mater. **31**, 2101796 (2021). https://doi.org/10.1002/adfm.202101796
34. Zhang, Y., Zhang, R., Chen, S.C., et al.: Diatomite-derived hierarchical porous crystalline-amorphous network for high-performance and sustainable Si anodes. Adv. Funct. Mater. **30**, 2005956 (2020). https://doi.org/10.1002/adfm.202005956
35. Fang, J.B., Cao, Y.Q., Chang, S.Z., et al.: Dual-design of nanoporous to compact interface via atomic/molecular layer deposition enabling a long-life silicon anode. Adv. Funct. Mater. **32**, 2109682 (2022). https://doi.org/10.1002/adfm.202109682
36. An, Y.L., Fei, H.F., Zeng, G.F., et al.: Green, scalable, and controllable fabrication of nanoporous silicon from commercial alloy precursors for high-energy lithium-ion batteries. ACS Nano **12**, 4993–5002 (2018). https://doi.org/10.1021/acsnano.8b02219
37. Zhao, C.H., Wada, T., De Andrade, V., et al.: Imaging of 3D morphological evolution of nanoporous silicon anode in lithium ion battery by X-ray nano-tomography. Nano Energy **52**, 381–390 (2018). https://doi.org/10.1016/j.nanoen.2018.08.009
38. Sohn, M., Lee, D.G., Park, H.I., et al.: Microstructure controlled porous silicon particles as a high capacity lithium

storage material via dual step pore engineering. Adv. Funct. Mater. **28**, 1800855 (2018). https://doi.org/10.1002/adfm.201800855
39. Zeng, Y.F., Huang, Y.D., Liu, N.T., et al.: N-doped porous carbon nanofibers sheathed pumpkin-like Si/C composites as free-standing anodes for lithium-ion batteries. J. Energy Chem. **54**, 727–735 (2021). https://doi.org/10.1016/j.jechem.2020.06.022
40. Yang, Z., Song, Y.W., Zhang, C.F., et al.: Porous 3D silicon-diamondyne blooms excellent storage and diffusion properties for Li, Na, and K ions. Adv. Energy Mater. **11**, 2101197 (2021). https://doi.org/10.1002/aenm.202101197
41. Yi, Z., Qian, Y., Cao, C.H., et al.: Porous Si/C microspheres decorated with stable outer carbon interphase and inner interpenetrated Si@C channels for enhanced lithium storage. Carbon **149**, 664–671 (2019). https://doi.org/10.1016/j.carbon.2019.04.080
42. Chen, S., Chen, Z., Xu, X.Y., et al.: Scalable 2D mesoporous silicon nanosheets for high-performance lithium-ion battery anode. Small **14**, e1703361 (2018). https://doi.org/10.1002/smll.201703361
43. Yi, Z., Lin, N., Xu, T.J., et al.: TiO_2 coated Si/C interconnected microsphere with stable framework and interface for high-rate lithium storage. Chem. Eng. J. **347**, 214–222 (2018). https://doi.org/10.1016/j.cej.2018.04.101
44. Yu, C.H., Lin, X.Q., Chen, X., et al.: Suppressing the side reaction by a selective blocking layer to enhance the performance of Si-based anodes. Nano Lett. **20**, 5176–5184 (2020). https://doi.org/10.1021/acs.nanolett.0c01394
45. Chen, Z.D., Li, L., Zhang, Z., et al.: "Sticky" carbon coating enables high-area-capacity lithium storage of silicon-graphitic carbon hybrid. Carbon **184**, 91–101 (2021). https://doi.org/10.1016/j.carbon.2021.07.097
46. Ning, L.J., Wu, Y.P., Wang, L.Z., et al.: Carbon anode materials from polysiloxanes for lithium ion batteries. J. Solid State Electrochem. **9**, 520–523 (2005). https://doi.org/10.1007/s10008-004-0616-8
47. Zhang, T., Fu, L.J., Gao, J., et al.: Core-shell Si/C nanocomposite as anode material for lithium ion batteries. Pure Appl. Chem. **78**, 1889–1896 (2006). https://doi.org/10.1351/pac200678101889
48. Yang, Y.J., Wu, S.X., Zhang, Y.P., et al.: Towards efficient binders for silicon based lithium-ion battery anodes. Chem. Eng. J. **406**, 126807 (2021). https://doi.org/10.1016/j.cej.2020.126807
49. Li, Z.H., Zhang, Y.P., Liu, T.F., et al.: Silicon anode with high initial coulombic efficiency by modulated trifunctional binder for high-areal-capacity lithium-ion batteries. Adv. Energy Mater. **10**, 1903110 (2020). https://doi.org/10.1002/aenm.201903110
50. Munao, D., van Erven, J.W.M., Valvo, M., et al.: Role of the binder on the failure mechanism of Si nano-composite electrodes for Li-ion batteries. J. Power Sources **196**, 6695–6702 (2011). https://doi.org/10.1016/j.jpowsour.2010.11.072
51. Li, Z.H., Wan, Z.W., Zeng, X.Q., et al.: A robust network binder via localized linking by small molecules for high-areal-capacity silicon anodes in lithium-ion batteries. Nano Energy **79**, 105430 (2021). https://doi.org/10.1016/j.nanoen.2020.105430
52. Li, S., Liu, Y.M., Zhang, Y.C., et al.: A review of rational design and investigation of binders applied in silicon-based anodes for lithium-ion batteries. J. Power Sources **485**, 229331 (2021). https://doi.org/10.1016/j.jpowsour.2020.229331
53. Chen, H., Wu, Z.Z., Su, Z., et al.: A mechanically robust self-healing binder for silicon anode in lithium ion batteries. Nano Energy **81**, 105654 (2021). https://doi.org/10.1016/j.nanoen.2020.105654
54. Liu, X.J., Xu, Z.X., Iqbal, A., et al.: Chemical coupled PEDOT:PSS/Si electrode: suppressed electrolyte consumption enables long-term stability. Nano Micro Lett. **13**, 54 (2021). https://doi.org/10.1007/s40820-020-00564-5
55. Ha, Y., Stetson, C., Harvey, S.P., et al.: Effect of water concentration in $LiPF_6$-based electrolytes on the formation, evolution, and properties of the solid electrolyte interphase on Si anodes. ACS Appl. Mater. Interfaces **12**, 49563–49573 (2020). https://doi.org/10.1021/acsami.0c12884
56. Cao, Z., Zheng, X.Y., Qu, Q.T., et al.: Electrolyte design enabling a high-safety and high-performance Si anode with a tailored electrode-electrolyte interphase. Adv. Mater. **33**, e2103178 (2021). https://doi.org/10.1002/adma.202103178
57. Wang, J.Y., Cui, Y.: Electrolytes for microsized silicon. Nat. Energy **5**, 361–362 (2020). https://doi.org/10.1038/s41560-020-0608-7
58. Xu, Z.X., Yang, J., Li, H.P., et al.: Electrolytes for advanced lithium ion batteries using silicon-based anodes. J. Mater. Chem. A **7**, 9432–9446 (2019). https://doi.org/10.1039/c9ta01876j
59. Chen, J., Fan, X.L., Li, Q., et al.: Electrolyte design for LiF-rich solid-electrolyte interfaces to enable high-performance microsized alloy anodes for batteries. Nat. Energy **5**, 386–397 (2020). https://doi.org/10.1038/s41560-020-0601-1
60. Shin, J., Kim, T.H., Lee, Y.J., et al.: Key functional groups defining the formation of Si anode solid-electrolyte interphase towards high energy density Li-ion batteries. Energy Storage Mater. **25**, 764–781 (2020). https://doi.org/10.1016/j.ensm.2019.09.009
61. Park, S., Jeong, S.Y., Lee, T.K., et al.: Replacing conventional battery electrolyte additives with dioxolone derivatives for high-energy-density lithium-ion batteries. Nat. Commun. **12**, 838 (2021). https://doi.org/10.1038/s41467-021-21106-6
62. Chung, D.J., Youn, D., Kim, S., et al.: Dehydrogenation-driven Li metal-free prelithiation for high initial efficiency SiO-based lithium storage materials. Nano Energy **89**, 106378 (2021). https://doi.org/10.1016/j.nanoen.2021.106378
63. Li, Y., Qian, Y., Zhou, J., et al.: Molten-LiCl induced thermochemical prelithiation of SiO_x: regulating the active Si/O ratio for high initial Coulombic efficiency. Nano Res. **15**, 230–237 (2022). https://doi.org/10.1007/s12274-021-3464-2
64. Zhan, R.M., Wang, X.C., Chen, Z.H., et al.: Promises and challenges of the practical implementation of prelithiation in lithium-ion batteries. Adv. Energy Mater. **11**, 2101565 (2021). https://doi.org/10.1002/aenm.202101565
65. Zhang, Y.X., Wu, B.R., Mu, G., et al.: Recent progress and perspectives on silicon anode: synthesis and prelithiation for LIBs energy storage. J. Energy Chem. **64**, 615–650 (2022). https://doi.org/10.1016/j.jechem.2021.04.013
66. Li, Y., Qian, Y., Zhao, Y., et al.: Revealing the interface-rectifying functions of a Li-cyanonaphthalene prelithiation system for SiO electrode. Sci. Bull. **67**, 636–645 (2022). https://doi.org/10.1016/j.scib.2021.12.010
67. Liu, Z.Z., Ma, S.B., Mu, X., et al.: A scalable cathode chemical prelithiation strategy for advanced silicon-based lithium ion full batteries. ACS Appl. Mater. Interfaces **13**, 11985–11994 (2021). https://doi.org/10.1021/acsami.0c22880
68. Choi, J., Jeong, H., Jang, J., et al.: Weakly solvating solution enables chemical prelithiation of graphite-SiO_x anodes for high-energy Li-ion batteries. J. Am. Chem. Soc. **143**, 9169–9176 (2021). https://doi.org/10.1021/jacs.1c03648
69. Liang, K., Huang, S.P., Zhao, H.S., et al.: An artificial interphase engineering simultaneously suppressing hydrogen evolution reaction and controlling zinc dendrite growth to achieve stable zinc metal anodes. Adv. Mater. Interfaces **9**, 2200564 (2022). https://doi.org/10.1002/admi.202200564
70. Ai, Q., Fang, Q.Y., Liang, J., et al.: Lithium-conducting covalent-organic-frameworks as artificial solid-electrolyte-interphase on silicon anode for high performance lithium ion batteries. Nano Energy **72**, 104657 (2020). https://doi.org/10.1016/j.nanoen.2020.104657

71. Li, G.J., Guo, S.G., Xiang, B., et al.: Recent advances and perspectives of microsized alloying-type porous anode materials in high-performance Li- and Na-ion batteries. Energy Mater. **2**, 200020 (2022). https://doi.org/10.20517/energymater.2022.24
72. Liu, X.H., Zheng, H., Zhong, L., et al.: Anisotropic swelling and fracture of silicon nanowires during lithiation. Nano Lett. **11**, 3312–3318 (2011). https://doi.org/10.1021/nl201684d
73. Stokes, K., Flynn, G., Geaney, H., et al.: Axial Si-Ge heterostructure nanowires as lithium-ion battery anodes. Nano Lett. **18**, 5569–5575 (2018). https://doi.org/10.1021/acs.nanolett.8b01988
74. Adkins, E.R., Jiang, T.Z., Luo, L.L., et al.: In situ transmission electron microsopy of oxide shell-induced pore formation in (de)lithiated silicon nanowires. ACS Energy Lett. **3**, 2829–2834 (2018). https://doi.org/10.1021/acsenergylett.8b01904
75. Ryu, I., Choi, J.W., Cui, Y., et al.: Size-dependent fracture of Si nanowire battery anodes. J. Mech. Phys. Solids **59**, 1717–1730 (2011). https://doi.org/10.1016/j.jmps.2011.06.003
76. He, T., Feng, J.R., Zhang, Y., et al.: Stress-relieved nanowires by silicon substitution for high-capacity and stable lithium storage. Adv. Energy Mater. **8**, 1702805 (2018). https://doi.org/10.1002/aenm.201702805
77. Sri Maha Vishnu, D., Sure, J., Kim, H.K., et al.: Solid state electrochemically synthesised β-SiC nanowires as the anode material in lithium ion batteries. Energy Storage Mater. **26**, 234–241 (2020). https://doi.org/10.1016/j.ensm.2019.12.041
78. Chang, H., Wu, Y.R., Han, X., et al.: Recent developments in advanced anode materials for lithium-ion batteries. Energy Mater. **1**, 100003 (2022). https://doi.org/10.20517/energymater.2021.02
79. Guo, J.P., Zhao, G.M., Xie, T., et al.: Carbon/polymer bilayer-coated Si-SiO_x electrodes with enhanced electrical conductivity and structural stability. ACS Appl. Mater. Interfaces **12**, 19023–19032 (2020). https://doi.org/10.1021/acsami.0c02445
80. Xu, Q., Sun, J.K., Yin, Y.X., et al.: Facile synthesis of blocky SiO_x/C with graphite-like structure for high-performance lithium-ion battery anodes. Adv. Funct. Mater. **28**, 1705235 (2018). https://doi.org/10.1002/adfm.201705235
81. Chen, W.Y., Xu, D.H., Kuang, S.J., et al.: Hierarchically porous SiO_x/C and carbon materials from one biomass waste precursor toward high-performance lithium/sodium storage. J. Power Sources **489**, 229459 (2021). https://doi.org/10.1016/j.jpowsour.2021.229459
82. Lee, J.H., Yoon, C.S., Hwang, J.Y., et al.: High-energy-density lithium-ion battery using a carbon-nanotube-Si composite anode and a compositionally graded $Li[Ni_{0.85}Co_{0.05}Mn_{0.10}]O_2$ cathode. Energy Environ. Sci. **9**, 2152–2158 (2016). https://doi.org/10.1039/c6ee01134a
83. Liu, R.P., Shen, C., Dong, Y., et al.: Sandwich-like CNTs/Si/C nanotubes as high performance anode materials for lithium-ion batteries. J. Mater. Chem. A **6**, 14797–14804 (2018). https://doi.org/10.1039/c8ta04686g
84. Ma, J., Sung, J., Lee, Y., et al.: Strategic pore architecture for accommodating volume change from high Si content in lithium-ion battery anodes. Adv. Energy Mater. **10**, 1903400 (2020). https://doi.org/10.1002/aenm.201903400
85. Lee, Y., Lee, T., Hong, J., et al.: Stress relief principle of micron-sized anodes with large volume variation for practical high-energy lithium-ion batteries. Adv. Funct. Mater. **30**, 2004841 (2020). https://doi.org/10.1002/adfm.202004841
86. Gao, X., Lu, W.Q., Xu, J.: Unlocking multiphysics design guidelines on Si/C composite nanostructures for high-energy-density and robust lithium-ion battery anode. Nano Energy **81**, 105591 (2021). https://doi.org/10.1016/j.nanoen.2020.105591
87. Ke, C.Z., Liu, F., Zheng, Z.M., et al.: Boosting lithium storage performance of Si nanoparticles via thin carbon and nitrogen/phosphorus co-doped two-dimensional carbon sheet dual encapsulation. Rare Met. **40**, 1347–1356 (2021). https://doi.org/10.1007/s12598-021-01716-1
88. Li, S., Niu, J.J., Zhao, Y.C., et al.: High-rate aluminium yolk-shell nanoparticle anode for Li-ion battery with long cycle life and ultrahigh capacity. Nat. Commun. **6**, 7872 (2015). https://doi.org/10.1038/ncomms8872
89. Ryu, J.H., Kim, J.W., Sung, Y.E., et al.: Failure modes of silicon powder negative electrode in lithium secondary batteries. Electrochem. Solid-State Lett. **7**, A306 (2004). https://doi.org/10.1149/1.1792242
90. Sun, L., Liu, Y.X., Shao, R., et al.: Recent progress and future perspective on practical silicon anode-based lithium ion batteries. Energy Storage Mater. **46**, 482–502 (2022). https://doi.org/10.1016/j.ensm.2022.01.042
91. Hwang, S.W., Yoon, W.Y.: Effect of Li powder-coated separator on irreversible behavior of SiO_x-C anode in lithium-ion batteries. J. Electrochem. Soc. **161**, A1753–A1758 (2014). https://doi.org/10.1149/2.0031412jes
92. Wang, G., Lu, Z.L., Li, Y., et al.: Electroceramics for high-energy density capacitors: current status and future perspectives. Chem. Rev. **121**, 6124–6172 (2021). https://doi.org/10.1021/acs.chemrev.0c01264
93. Zhang, Y.L., Mu, Z.J., Lai, J.P., et al.: MXene/Si@SiO_x@C layer-by-layer superstructure with autoadjustable function for superior stable lithium storage. ACS Nano (2019). https://doi.org/10.1021/acsnano.8b08821
94. Li, P., Hwang, J.Y., Sun, Y.K.: Nano/microstructured silicon-graphite composite anode for high-energy-density Li-ion battery. ACS Nano (2019). https://doi.org/10.1021/acsnano.9b00169
95. Kwon, H.J., Hwang, J.Y., Shin, H.J., et al.: Nano/microstructured silicon-carbon hybrid composite particles fabricated with corn starch biowaste as anode materials for Li-ion batteries. Nano Lett. **20**, 625–635 (2020). https://doi.org/10.1021/acs.nanolett.9b04395
96. Zeng, W.W., Wang, L., Peng, X., et al.: Enhanced ion conductivity in conducting polymer binder for high-performance silicon anodes in advanced lithium-ion batteries. Adv. Energy Mater. **8**, 1702314 (2018). https://doi.org/10.1002/aenm.201702314
97. Cao, L., Huang, T., Cui, M.Y., et al.: Facile and efficient fabrication of branched Si@C anode with superior electrochemical performance in LIBs. Small **17**, e2005997 (2021). https://doi.org/10.1002/smll.202005997
98. Zhao, H.S., Qi, Y.L., Liang, K., et al.: Interface-driven pseudocapacitance endowing sandwiched $CoSe_2$/N-doped carbon/TiO_2 microcubes with ultra-stable sodium storage and long-term cycling stability. ACS Appl. Mater. Interfaces **13**, 61555–61564 (2021). https://doi.org/10.1021/acsami.1c20154
99. Liang, K., Zhao, H.S., Li, J.B., et al.: Engineering crystal growth and surface modification of $Na_3V_2(PO_4)_2F_3$ cathode for high-energy-density sodium-ion batteries. Small **19**, e2207562 (2023). https://doi.org/10.1002/smll.202207562
100. Wang, Z.H., Zhao, H.S., Zhou, B., et al.: In situ surface coating and oxygen vacancy dual strategy endowing a Li-rich $Li_{1.2}Mn_{0.55}Ni_{0.11}Co_{0.14}O_2$ cathode with superior lithium storage performance. ACS Appl. Energy Mater. **6**, 387–396 (2023). https://doi.org/10.1021/acsaem.2c03301
101. Liang, K., Wu, D.X., Ren, Y.R., et al.: Research progress on $Na_3V_2(PO_4)_2F_3$-based cathode materials for sodium-ion batteries. Chin. Chem. Lett. **34**, 107978 (2023). https://doi.org/10.1016/j.cclet.2022.107978
102. Chen, C.G., Zhou, T., Danilov, D.L., et al.: Impact of dual-layer solid-electrolyte interphase inhomogeneities on early-stage defect formation in Si electrodes. Nat. Commun. **11**, 3283 (2020). https://doi.org/10.1038/s41467-020-17104-9
103. Zhao, H.S., Liang, K., Wang, S.J., et al.: A stress self-adaptive silicon/carbon "ordered structures" to suppress the electro-chemo-mechanical failure: piezo-electrochemistry and

piezo-ionic dynamics. Adv. Sci. **10**, 2303696 (2023). https://doi.org/10.1002/advs.202303696
104. Peled, E., Menkin, S.: Review—SEI: past, present and future. J. Electrochem. Soc. **164**, A1703–A1719 (2017). https://doi.org/10.1149/2.1441707jes
105. Zhao, H.S., Zhong, J.J., Qi, Y.L., et al.: 90 C fast-charge Na-ion batteries for pseudocapacitive faceted TiO_2 anodes based on robust interface chemistry. Chem. Eng. J. **465**, 143032 (2023). https://doi.org/10.1016/j.cej.2023.143032
106. Zhao, H.S., Qi, Y.L., Liang, K., et al.: Phosphorus-doping and oxygen vacancy endowing anatase TiO_2 with excellent sodium storage performance. Rare Met. **41**, 1284–1293 (2022). https://doi.org/10.1007/s12598-021-01864-4
107. Yang, G., Frisco, S., Tao, R.M., et al.: Robust solid/electrolyte interphase (SEI) formation on Si anodes using glyme-based electrolytes. ACS Energy Lett. **6**, 1684–1693 (2021). https://doi.org/10.1021/acsenergylett.0c02629
108. Nie, M.Y., Abraham, D.P., Chen, Y.J., et al.: Silicon solid electrolyte interphase (SEI) of lithium ion battery characterized by microscopy and spectroscopy. J. Phys. Chem. C **117**, 13403–13412 (2013). https://doi.org/10.1021/jp404155y
109. Wu, H., Chan, G., Choi, J.W., et al.: Stable cycling of double-walled silicon nanotube battery anodes through solid-electrolyte interphase control. Nat. Nanotechnol. **7**, 310–315 (2012). https://doi.org/10.1038/nnano.2012.35
110. Chen, Z.D., Soltani, A., Chen, Y.G., et al.: Emerging organic surface chemistry for Si anodes in lithium-ion batteries: advances, prospects, and beyond. Adv. Energy Mater. **12**, 2200924 (2022). https://doi.org/10.1002/aenm.202200924
111. Kumar, R., Tokranov, A., Sheldon, B.W., et al.: In situ and operando investigations of failure mechanisms of the solid electrolyte interphase on silicon electrodes. ACS Energy Lett. **1**, 689–697 (2016). https://doi.org/10.1021/acsenergylett.6b00284
112. Dou, F., Weng, Y.H., Wang, Q.Y., et al.: In situ imaging analysis of the inhibition effect of functional coating on the volume expansion of silicon anodes. Chem. Eng. J. **417**, 128122 (2021). https://doi.org/10.1016/j.cej.2020.128122
113. Parekh, M.H., Sediako, A.D., Naseri, A., et al.: In situ mechanistic elucidation of superior Si-C-graphite Li-ion battery anode formation with thermal safety aspects. Adv. Energy Mater. **10**, 1902799 (2020). https://doi.org/10.1002/aenm.201902799
114. Liu, X.H., Huang, J.Y.: In situ TEM electrochemistry of anode materials in lithium ion batteries. Energy Environ. Sci. **4**, 3844 (2011). https://doi.org/10.1039/c1ee01918j
115. Liu, J., Yuan, H., Liu, H., et al.: Unlocking the failure mechanism of solid state lithium metal batteries. Adv. Energy Mater. **12**, 2100748 (2022). https://doi.org/10.1002/aenm.202100748
116. Zhou, Y.Z., Yang, Y.J., Hou, G.L., et al.: Stress-relieving defects enable ultra-stable silicon anode for Li-ion storage. Nano Energy **70**, 104568 (2020). https://doi.org/10.1016/j.nanoen.2020.104568
117. Finegan, D.P., Vamvakeros, A., Cao, L., et al.: Spatially resolving lithiation in silicon-graphite composite electrodes via in situ high-energy X-ray diffraction computed tomography. Nano Lett. **19**, 3811–3820 (2019). https://doi.org/10.1021/acs.nanolett.9b00955
118. Zhang, Z.Q., Wang, H.Q., Cheng, M.J., et al.: Confining invasion directions of Li^+ to achieve efficient Si anode material for lithium-ion batteries. Energy Storage Mater. **42**, 231–239 (2021). https://doi.org/10.1016/j.ensm.2021.07.036
119. Zhou, J., Zhao, H.Y., Lin, N., et al.: Silicothermic reduction reaction for fabricating interconnected Si-Ge nanocrystals with fast and stable Li-storage. J. Mater. Chem. A **8**, 6597–6606 (2020). https://doi.org/10.1039/d0ta00109k
120. Wang, J., Yang, Z., Mao, B.G., et al.: Transgenic engineering on silicon surfaces enables robust interface chemistry. ACS Energy Lett. **7**, 2781–2791 (2022). https://doi.org/10.1021/acsenergylett.2c01202
121. Liu, J., Lee, S.Y., Yoo, J., et al.: Real-time observation of mechanical evolution of micro-sized Si anodes by in situ atomic force microscopy. ACS Mater. Lett. **4**, 840–846 (2022). https://doi.org/10.1021/acsmaterialslett.2c00059
122. Lindgren, F., Xu, C., Niedzicki, L., et al.: SEI formation and interfacial stability of a Si electrode in a LiTDI-salt based electrolyte with FEC and VC additives for Li-ion batteries. ACS Appl. Mater. Interfaces **8**, 15758–15766 (2016). https://doi.org/10.1021/acsami.6b02650
123. Young, B.T., Nguyen, C.C., Lobach, A., et al.: Role of binders in solid electrolyte interphase formation in lithium ion batteries studied with hard X-ray photoelectron spectroscopy. J. Mater. Res. **34**, 97–106 (2019). https://doi.org/10.1557/jmr.2018.363
124. Mu, T.S., Zhao, Y., Zhao, C.T., et al.: Stable silicon anodes by molecular layer deposited artificial zincone coatings. Adv. Funct. Mater. **31**, 2010526 (2021). https://doi.org/10.1002/adfm.202010526
125. Zhou, J.G., Hu, Y.F., Li, X.L., et al.: Chemical bonding in amorphous Si-coated carbon nanotubes as anodes for Li ion batteries: a XANES study. RSC Adv. **4**, 20226–20229 (2014). https://doi.org/10.1039/c4ra01332h
126. Xu, S., Zhou, J.G., Wang, J., et al.: In situ synthesis of graphene-coated silicon monoxide anodes from coal-derived humic acid for high-performance lithium-ion batteries. Adv. Funct. Mater. **31**, 2101645 (2021). https://doi.org/10.1002/adfm.202101645
127. Jeschull, F., Lindgren, F., Lacey, M.J., et al.: Influence of inactive electrode components on degradation phenomena in nano-Si electrodes for Li-ion batteries. J. Power Sources **325**, 513–524 (2016). https://doi.org/10.1016/j.jpowsour.2016.06.059
128. Hirata, A., Kohara, S., Asada, T., et al.: Atomic-scale disproportionation in amorphous silicon monoxide. Nat. Commun. **7**, 11591 (2016). https://doi.org/10.1038/ncomms11591
129. Kitada, K., Pecher, O., Magusin, P.C.M.M., et al.: Unraveling the reaction mechanisms of SiO anodes for Li-ion batteries by combining in situ ^{7}Li and ex situ ^{7}Li/^{29}Si solid-state NMR spectroscopy. J. Am. Chem. Soc. **141**, 7014–7027 (2019). https://doi.org/10.1021/jacs.9b01589
130. Huang, W., Wang, J.Y., Braun, M.R., et al.: Dynamic structure and chemistry of the silicon solid-electrolyte interphase visualized by cryogenic electron microscopy. Matter **1**, 1232–1245 (2019). https://doi.org/10.1016/j.matt.2019.09.020
131. Zhang, X., Weng, S.T., Yang, G.J., et al.: Interplay between solid-electrolyte interphase and (in)active Li_xSi in silicon anode. Cell Rep. Phys. Sci. **2**, 100668 (2021). https://doi.org/10.1016/j.xcrp.2021.100668
132. Zhu, R.Y., Wang, Z.H., Hu, X.J., et al.: Silicon in hollow carbon nanospheres assembled microspheres cross-linked with N-doped carbon fibers toward a binder free, high performance, and flexible anode for lithium-ion batteries. Adv. Funct. Mater. **31**, 2101487 (2021). https://doi.org/10.1002/adfm.202101487
133. Ren, Y., Yin, X.C., Xiao, R., et al.: Layered porous silicon encapsulated in carbon nanotube cage as ultra-stable anode for lithium-ion batteries. Chem. Eng. J. **431**, 133982 (2022). https://doi.org/10.1016/j.cej.2021.133982
134. Kang, M.S., Heo, I., Kim, S., et al.: High-areal-capacity of micron-sized silicon anodes in lithium-ion batteries by using wrinkled-multilayered-graphenes. Energy Storage Mater. **50**, 234–242 (2022). https://doi.org/10.1016/j.ensm.2022.05.025
135. Qi, Y., Wang, G., Li, S., et al.: Recent progress of structural designs of silicon for performance-enhanced lithium-ion batteries. Chem. Eng. J. **397**, 125380 (2020). https://doi.org/10.1016/j.cej.2020.125380

136. Zhang, J., Zuo, S.L., Wang, Y.Q., et al.: Scalable synthesis of interconnected hollow Si/C nanospheres enabled by carbon dioxide in magnesiothermic reduction for high-performance lithium energy storage. J. Power Sources **495**, 229803 (2021). https://doi.org/10.1016/j.jpowsour.2021.229803
137. Gao, J.F., Zuo, S.L., Liu, H., et al.: An interconnected and scalable hollow Si-C nanospheres/graphite composite for high-performance lithium-ion batteries. J. Colloid Interface Sci. **624**, 555–563 (2022). https://doi.org/10.1016/j.jcis.2022.05.135
138. Zhou, X.M., Liu, Y., Ren, Y., et al.: Engineering molecular polymerization for template-free SiO_x/C hollow spheres as ultrastable anodes in lithium-ion batteries. Adv. Funct. Mater. **31**, 2101145 (2021). https://doi.org/10.1002/adfm.202101145
139. Chae, S., Xu, Y.B., Yi, R., et al.: A micrometer-sized silicon/carbon composite anode synthesized by impregnation of petroleum pitch in nanoporous silicon. Adv. Mater. **33**, 2103095 (2021). https://doi.org/10.1002/adma.202103095
140. Liu, Q., Ji, Y.X., Yin, X.M., et al.: Magnesiothermic reduction improved route to high-yield synthesis of interconnected porous Si@C networks anode of lithium ions batteries. Energy Storage Mater. **46**, 384–393 (2022). https://doi.org/10.1016/j.ensm.2021.12.017
141. Kim, H., Baek, J., Son, D.K., et al.: Hollow porous N and Co dual-doped silicon@carbon nanocube derived by ZnCo-bimetallic metal-organic framework toward advanced lithium-ion battery anodes. ACS Appl. Mater. Interfaces **14**, 45458–45475 (2022). https://doi.org/10.1021/acsami.2c13607
142. Yang, Z.W., Wu, C., Li, S., et al.: A unique structure of highly stable interphase and self-consistent stress distribution radial-gradient porous for silicon anode. Adv. Funct. Mater. **32**, 2107897 (2022). https://doi.org/10.1002/adfm.202107897
143. Shi, J.W., Gao, H.Y., Hu, G.X., et al.: Interfacial self-assembled Si@SiO@C microclusters with high tap density for high-performance Li-ion batteries. Mater. Today Energy **29**, 101090 (2022). https://doi.org/10.1016/j.mtener.2022.101090
144. Liu, Z.G., Lu, D.Z., Wang, W., et al.: Integrating dually encapsulated Si architecture and dense structural engineering for ultrahigh volumetric and areal capacity of lithium storage. ACS Nano **16**, 4642–4653 (2022). https://doi.org/10.1021/acsnano.1c11298
145. Tian, Y.F., Li, G., Xu, D.X., et al.: Micrometer-sized $SiMg_yO_x$ with stable internal structure evolution for high-performance Li-ion battery anodes. Adv. Mater. **34**, 2200672 (2022). https://doi.org/10.1002/adma.202200672
146. An, W.L., He, P., Che, Z.Z., et al.: Scalable synthesis of pore-rich Si/C@C core-shell-structured microspheres for practical long-life lithium-ion battery anodes. ACS Appl. Mater. Interfaces **14**, 10308–10318 (2022). https://doi.org/10.1021/acsami.1c22656
147. An, Y.L., Tian, Y., Liu, C.K., et al.: One-step, vacuum-assisted construction of micrometer-sized nanoporous silicon confined by uniform two-dimensional N-doped carbon toward advanced Li ion and MXene-based Li metal batteries. ACS Nano **16**, 4560–4577 (2022). https://doi.org/10.1021/acsnano.1c11098
148. Fan, Z.Q., Wang, Y.T., Zheng, S.S., et al.: A submicron Si@C core-shell intertwined with carbon nanowires and graphene nanosheet as a high-performance anode material for lithium ion battery. Energy Storage Mater. **39**, 1–10 (2021). https://doi.org/10.1016/j.ensm.2021.04.005
149. Luo, H., Zhang, X.M., Xu, C., et al.: Constructing a yolk-shell structure SiO_x/C@C composite for long-life lithium-ion batteries. ACS Appl. Energy Mater. **5**, 8982–8989 (2022). https://doi.org/10.1021/acsaem.2c01463
150. Wang, J., Gao, C.H., Yang, Z., et al.: Carbon-coated mesoporous silicon shell-encapsulated silicon nano-grains for high performance lithium-ion batteries anode. Carbon **192**, 277–284 (2022). https://doi.org/10.1016/j.carbon.2022.02.063
151. Li, J.X., Huang, Y.C., Huang, W.J., et al.: Simple designed micro-nano Si-graphite hybrids for lithium storage. Small **17**, 2006373 (2021). https://doi.org/10.1002/smll.202006373
152. Dai, X.Q., Liu, H.T., Liu, X., et al.: Silicon nanoparticles encapsulated in multifunctional crosslinked nano-silica/carbon hybrid matrix as a high-performance anode for Li-ion batteries. Chem. Eng. J. **418**, 129468 (2021). https://doi.org/10.1016/j.cej.2021.129468
153. Zhou, Y., Feng, S.H., Zhu, P.F., et al.: Self-sacrificial-reaction guided formation of hierarchical electronic/ionic conductive shell enabling high-performance nano-silicon anode. Chem. Eng. J. **415**, 128998 (2021). https://doi.org/10.1016/j.cej.2021.128998
154. Zhang, J.Y., Hou, Z.L., Zhang, X.M., et al.: Si@Cu composite anode material prepared by magnetron sputtering for high-capacity lithium-ion batteries. Int. J. Hydrog. Energy **47**, 4766–4771 (2022). https://doi.org/10.1016/j.ijhydene.2021.11.080
155. Wang, Z.Y., Xu, Z.G., Yuan, Y.P., et al.: Microspheres comprise Si nanoparticles modified with TiO_2 and wrapped by graphene as high-performance anode for lithium-ion batteries. Appl. Surf. Sci. **598**, 153790 (2022). https://doi.org/10.1016/j.apsusc.2022.153790
156. Li, X.D., Zhao, Y.M., Tian, Y.F., et al.: Lithium/boron Co-doped micrometer SiO_x as promising anode materials for high-energy-density Li-ion batteries. ACS Appl. Mater. Interfaces **14**, 27854–27860 (2022). https://doi.org/10.1021/acsami.2c04983
157. Chen, J.Y., Zhao, H.S., Li, J.B., et al.: Piezoelectric-driven self-accelerated anion migration for SiO_X-C/$PbZr_{0.52}Ti_{0.48}O_3$ with durable lithium storage performance. Ceram. Int. **48**, 11257–11264 (2022). https://doi.org/10.1016/j.ceramint.2021.12.346
158. Zhong, J., Wang, T., Wang, L., et al.: A silicon monoxide lithium-ion battery anode with ultrahigh areal capacity. Nano Micro Lett. **14**, 50 (2022). https://doi.org/10.1007/s40820-022-00790-z
159. Jeong, W.J., Chung, D.J., Youn, D., et al.: Double-buffer-phase embedded Si/$TiSi_2$/Li_2SiO_3 nanocomposite lithium storage materials by phase-selective reaction of SiO with metal hydrides. Energy Storage Mater. **50**, 740–750 (2022). https://doi.org/10.1016/j.ensm.2022.06.023
160. Adhitama, E., Dias Brandao, F., Dienwiebel, I., et al.: Prelithiation of silicon anodes by thermal evaporation of lithium for boosting the energy density of lithium ion cells. Adv. Funct. Mater. **32**, 2201455 (2022). https://doi.org/10.1002/adfm.202201455
161. Ai, Q., Li, D.P., Guo, J.G., et al.: Artificial solid electrolyte interphase coating to reduce lithium trapping in silicon anode for high performance lithium-ion batteries. Adv. Mater. Interfaces **6**, 1901187 (2019). https://doi.org/10.1002/admi.201901187
162. Yan, J.W., Zhao, X.L., He, S.G., et al.: Artificial solid electrolyte interphase coating to reduce lithium trapping in silicon anode for highly stable lithium storage. Surf. Interfaces **31**, 102029 (2022). https://doi.org/10.1016/j.surfin.2022.102029
163. Wu, K., Yi, J., Liu, X.Y., et al.: Regulating Zn deposition via an artificial solid-electrolyte interface with aligned dipoles for long life Zn anode. Nano Micro Lett. **13**, 79 (2021). https://doi.org/10.1007/s40820-021-00599-2
164. Li, Y.Z., Lu, J.M., Wang, Z.Y., et al.: Suppressing continuous volume expansion of Si nanoparticles by an artificial solid electrolyte interphase for high-performance lithium-ion batteries. ACS Sustain. Chem. Eng. **9**, 8059–8068 (2021). https://doi.org/10.1021/acssuschemeng.0c08964
165. Chen, C.C., Fu, L.J., Maier, J.: Synergistic, ultrafast mass storage and removal in artificial mixed conductors. Nature **536**, 159–164 (2016). https://doi.org/10.1038/nature19078
166. Cao, Z., Zheng, X.Y., Wang, Y., et al.: Tailoring a multifunctional, boron and fluoride-enriched solid-electrolyte interphase precursor towards high-rate and stable-cycling silicon anodes.

Nano Energy **93**, 106811 (2022). https://doi.org/10.1016/j.nanoen.2021.106811
167. Deng, L., Deng, S.S., Pan, S.Y., et al.: Multivalent amide-hydrogen-bond supramolecular binder enhances the cyclic stability of silicon-based anodes for lithium-ion batteries. ACS Appl. Mater. Interfaces **13**, 22567–22576 (2021). https://doi.org/10.1021/acsami.1c04501
168. Ling, L.M., Bai, Y., Wang, Z.H., et al.: Remarkable effect of sodium alginate aqueous binder on anatase TiO_2 as high-performance anode in sodium ion batteries. ACS Appl. Mater. Interfaces **10**, 5560–5568 (2018). https://doi.org/10.1021/acsami.7b17659
169. Bhati, M., Nguyen, Q.A., Biswal, S.L., et al.: Combining ReaxFF simulations and experiments to evaluate the structure-property characteristics of polymeric binders in Si-based Li-ion batteries. ACS Appl. Mater. Interfaces **13**, 41956–41967 (2021). https://doi.org/10.1021/acsami.1c08484
170. Kim, J., Park, Y.K., Kim, H., et al.: Ambidextrous polymeric binder for silicon anodes in lithium-ion batteries. Chem. Mater. **34**, 5791–5798 (2022). https://doi.org/10.1021/acs.chemmater.2c00220
171. Rajeev, K.K., Jang, W., Kim, S., et al.: Chitosan-grafted-gallic acid as a nature-inspired multifunctional binder for high-performance silicon anodes in lithium-ion batteries. ACS Appl. Energy Mater. **5**, 3166–3178 (2022). https://doi.org/10.1021/acsaem.1c03791
172. Xue, S.D., Fu, Y.D., Song, Z.B., et al.: Coil-to-stretch transition of binder chains enabled by "nano-combs" to facilitate highly stable SiO_x anode. Energy Environ. Mater. **5**, 1310–1316 (2022). https://doi.org/10.1002/eem2.12248
173. Zhang, S., Xu, X., Tu, J., et al.: Cross-linked binder enables reversible volume changes of Si-based anodes from sustainable photovoltaic waste silicon. Mater. Today Sustain. **19**, 100178 (2022). https://doi.org/10.1016/j.mtsust.2022.100178
174. Xiao, H.Y., Qiu, J.C., Wu, S.X., et al.: Cross-linked γ-polyglutamic acid as an aqueous SiO_x anode binder for long-term lithium-ion batteries. ACS Appl. Mater. Interfaces **14**, 18625–18633 (2022). https://doi.org/10.1021/acsami.2c03458
175. Lin, S., Wang, F.F., Hong, R.Y.: Polyacrylic acid and β-cyclodextrin polymer cross-linking binders to enhance capacity performance of silicon/carbon composite electrodes in lithium-ion batteries. J. Colloid Interface Sci. **613**, 857–865 (2022). https://doi.org/10.1016/j.jcis.2022.01.040
176. Weng, Z., Di, S.H., Chen, L., et al.: Random copolymer hydrogel as elastic binder for the SiO_x microparticle anode in lithium-ion batteries. ACS Appl. Mater. Interfaces **14**, 42494–42503 (2022). https://doi.org/10.1021/acsami.2c12128
177. Pan, H.W., Xu, Z.S., Wei, Z.Y., et al.: Synergistic double cross-linked dynamic network of epoxidized natural rubber/glycinamide modified polyacrylic acid for silicon anode in lithium ion battery: high peel strength and super cycle stability. ACS Appl. Mater. Interfaces **14**, 33315–33327 (2022). https://doi.org/10.1021/acsami.2c08038
178. Chen, H., Ling, M., Hencz, L., et al.: Exploring chemical, mechanical, and electrical functionalities of binders for advanced energy-storage devices. Chem. Rev. **118**, 8936–8982 (2018). https://doi.org/10.1021/acs.chemrev.8b00241
179. Wang, H.L., Wu, B.Z., Wu, X.K., et al.: Key factors for binders to enhance the electrochemical performance of silicon anodes through molecular design. Small **18**, 2101680 (2022). https://doi.org/10.1002/smll.202101680
180. Jiang, M.F., Mu, P.Z., Zhang, H.R., et al.: An endotenon sheath-inspired double-network binder enables superior cycling performance of silicon electrodes. Nano Micro Lett. **14**, 87 (2022). https://doi.org/10.1007/s40820-022-00833-5
181. Xiong, J.H., Dupré, N., Moreau, P., et al.: From the direct observation of a PAA-based binder using STEM-VEELS to the ageing mechanism of silicon/graphite anode with high areal capacity cycled in an FEC-rich and EC-free electrolyte. Adv. Energy Mater. **12**, 2103348 (2022). https://doi.org/10.1002/aenm.202103348
182. Kim, J., Choi, J., Park, K., et al.: Host-guest interlocked complex binder for silicon-graphite composite electrodes in lithium ion batteries. Adv. Energy Mater. **12**, 2103718 (2022). https://doi.org/10.1002/aenm.202103718
183. Gendensuren, B., Sugartseren, N., Kim, M., et al.: Incorporation of aniline tetramer into alginate-grafted-polyacrylamide as polymeric binder for high-capacity silicon/graphite anodes. Chem. Eng. J. **433**, 133553 (2022). https://doi.org/10.1016/j.cej.2021.133553
184. Pan, S.Y., Han, J.W., Wang, Y.Q., et al.: Integrating SEI into layered conductive polymer coatings for ultrastable silicon anodes. Adv. Mater. **34**, 2203617 (2022). https://doi.org/10.1002/adma.202203617
185. Liu, H.M., Wu, Q.P., Guan, X., et al.: Ionically conductive self-healing polymer binders with poly(ether-thioureas) segments for high-performance silicon anodes in lithium-ion batteries. ACS Appl. Energy Mater. **5**, 4934–4944 (2022). https://doi.org/10.1021/acsaem.2c00329
186. Jang, W., Rajeev, K.K., Thorat, G.M., et al.: Lambda carrageenan as a water-soluble binder for silicon anodes in lithium-ion batteries. ACS Sustain. Chem. Eng. **10**, 12620–12629 (2022). https://doi.org/10.1021/acssuschemeng.2c03313
187. Niesen, S., Fox, A., Murugan, S., et al.: Multifunctional self-cross-linked copolymer binder for high-loading silicon anodes. ACS Appl. Energy Mater. **5**, 11386–11391 (2022). https://doi.org/10.1021/acsaem.2c01867
188. Chen, H., Wu, Z.Z., Su, Z., et al.: A hydrophilic poly(methyl vinyl ether-alt-maleic acid) polymer as a green, universal, and dual-functional binder for high-performance silicon anode and sulfur cathode. J. Energy Chem. **62**, 127–135 (2021). https://doi.org/10.1016/j.jechem.2021.03.015
189. Deng, L., Zheng, Y., Zheng, X.M., et al.: Design criteria for silicon-based anode binders in half and full cells. Adv. Energy Mater. **12**, 2200850 (2022). https://doi.org/10.1002/aenm.202200850
190. Song, Z.B., Zhang, T.H., Wang, L., et al.: Bio-inspired binder design for a robust conductive network in silicon-based anodes. Small Meth. **6**, 2101591 (2022). https://doi.org/10.1002/smtd.202101591
191. Li, Z.H., Wu, G., Yang, Y.J., et al.: An ion-conductive grafted polymeric binder with practical loading for silicon anode with high interfacial stability in lithium-ion batteries. Adv. Energy Mater. **12**, 2201197 (2022). https://doi.org/10.1002/aenm.202201197
192. Kim, J., Kim, M.S., Lee, Y., et al.: Hierarchically structured conductive polymer binders with silver nanowires for high-performance silicon anodes in lithium-ion batteries. ACS Appl. Mater. Interfaces **14**, 17340–17347 (2022). https://doi.org/10.1021/acsami.2c00844
193. Shi, Z.X., Liu, Q., Yang, Z.Z., et al.: A chemical switch enabled autonomous two-stage crosslinking polymeric binder for high performance silicon anodes. J. Mater. Chem. A **10**, 1380–1389 (2022). https://doi.org/10.1039/d1ta07112b
194. Hu, L.L., Jin, M.H., Zhang, Z., et al.: Interface-adaptive binder enabled by supramolecular interactions for high-capacity Si/C composite anodes in lithium-ion batteries. Adv. Funct. Mater. **32**, 2111560 (2022). https://doi.org/10.1002/adfm.202111560
195. Liu, Z.M., Fang, C., He, X., et al.: In situ-formed novel elastic network binder for a silicon anode in lithium-ion batteries.

ACS Appl. Mater. Interfaces **13**, 46518–46525 (2021). https://doi.org/10.1021/acsami.1c09607
196. Zhao, J.K., Wei, D.N., Wang, J.J., et al.: Inorganic crosslinked supramolecular binder with fast self-healing for high performance silicon based anodes in lithium-ion batteries. J. Colloid Interface Sci. **625**, 373–382 (2022). https://doi.org/10.1016/j.jcis.2022.06.002
197. Lee, H.A., Shin, M., Kim, J., et al.: Designing adaptive binders for microenvironment settings of silicon anode particles. Adv. Mater. **33**, 2007460 (2021). https://doi.org/10.1002/adma.202007460
198. Parfeneva, A.V., Rumyantsev, A.M., Lozhkina, D.A., et al.: Influence of fluoroethylene carbonate in the composition of an aprotic electrolyte on the electrochemical characteristics of LIB's anodes based on carbonized nanosilicon. Batteries **8**, 91 (2022). https://doi.org/10.3390/batteries8080091
199. Cao, X., Jia, H., Xu, W., et al.: Review—localized high-concentration electrolytes for lithium batteries. J. Electrochem. Soc. **168**, 010522 (2021). https://doi.org/10.1149/1945-7111/abd60e
200. Huang, W.B., Wang, Y., Lv, L.Z., et al.: 1-Hydroxyethylidene-1,1-diphosphonic acid: a multifunctional interface modifier for eliminating HF in silicon anode. Energy Storage Mater. **42**, 493–501 (2021). https://doi.org/10.1016/j.ensm.2021.08.010
201. Tan, T., Lee, P.K., Marium, M., et al.: (3-Aminopropyl)triethoxysilane as an electrolyte additive for enhancing the thermal stability of silicon anode in lithium-ion batteries. ACS Appl. Energy Mater. **5**, 11254–11262 (2022). https://doi.org/10.1021/acsaem.2c01816
202. Chen, H., Adekoya, D., Hencz, L., et al.: Stable seamless interfaces and rapid ionic conductivity of Ca-CeO_2/LiTFSI/PEO composite electrolyte for high-rate and high-voltage all-solid-state battery. Adv. Energy Mater. **10**, 2000049 (2020). https://doi.org/10.1002/aenm.202000049
203. Salah, M., Pathirana, T., de Eulate, E.A., et al.: Effect of vinylene carbonate electrolyte additive and battery cycling protocol on the electrochemical and cyclability performance of silicon thin-film anodes. J. Energy Storage **46**, 103868 (2022). https://doi.org/10.1016/j.est.2021.103868
204. Ha, Y., Martin, T.R., Frisco, S., et al.: Evaluating the effect of electrolyte additive functionalities on NMC622/Si cell performance. J. Electrochem. Soc. **169**, 070515 (2022). https://doi.org/10.1149/1945-7111/ac7e75
205. Chen, H., Zheng, M.T., Qian, S.S., et al.: Functional additives for solid polymer electrolytes in flexible and high-energy-density solid-state lithium-ion batteries. Carbon Energy **3**, 929–956 (2021). https://doi.org/10.1002/cey2.146
206. Wen, Z.Y., Wu, F., Li, L., et al.: Electrolyte design enabling stable solid electrolyte interface for high-performance silicon/carbon anodes. ACS Appl. Mater. Interfaces **14**, 38807–38814 (2022). https://doi.org/10.1021/acsami.2c09997
207. Duan, K.J., Ning, J.R., Zhou, L., et al.: Synergistic inorganic-organic dual-additive electrolytes enable practical high-voltage lithium-ion batteries. ACS Appl. Mater. Interfaces **14**, 10447–10456 (2022). https://doi.org/10.1021/acsami.1c24808
208. He, S.G., Huang, S.M., Zhao, Y., et al.: Design of a dual-electrolyte battery system based on a high-energy NCM811-Si/C full battery electrode-compatible electrolyte. ACS Appl. Mater. Interfaces **13**, 54069–54078 (2021). https://doi.org/10.1021/acsami.1c17841
209. Li, Q., Li, Y., Wang, Y.W., et al.: Achieving fast ionic conductivity and high electrochemical stability through polyhedral structure design. Energy Storage Mater. **47**, 70–78 (2022). https://doi.org/10.1016/j.ensm.2022.01.050
210. Fuller, E.J., Strelcov, E., Weaver, J.L., et al.: Spatially resolved potential and Li-ion distributions reveal performance-limiting regions in solid-state batteries. ACS Energy Lett. **6**, 3944–3951 (2021). https://doi.org/10.1021/acsenergylett.1c01960
211. Yu, Z.Z., Zhou, L.H., Cheng, Y., et al.: Preset lithium source electrolyte boosts SiO anode performance for lithium-ion batteries. ACS Sustain. Chem. Eng. **10**, 10351–10360 (2022). https://doi.org/10.1021/acssuschemeng.2c03081
212. Kwon, J., Kim, J., Bae, S.Y., et al.: Polyanion-assisted ionic-electronic conductive agents designed for high density Si-based anodes. J. Power Sources **541**, 231728 (2022). https://doi.org/10.1016/j.jpowsour.2022.231728
213. Haridas, A.K., Nguyen, Q.A., Terlier, T., et al.: Investigating the compatibility of TTMSP and FEC electrolyte additives for $LiNi_{0.5}Mn_{0.3}Co_{0.2}O_2$ (NMC)-silicon lithium-ion batteries. ACS Appl. Mater. Interfaces **13**, 2662–2673 (2021). https://doi.org/10.1021/acsami.0c19347

Hongshun Zhao is currently a Ph.D. student under the supervision of Prof. Yurong Ren in School of Materials Science and Engineering at Changzhou University. He received his Master Degree in materials engineering from Changzhou University in 2022. His current research topic focuses on the Si-based anode materials for lithium-ion batteries and beyond, mainly focusing on understanding the structural and interfacial properties of the Si-based anode materials.

Jianbin Li is currently serving as a lecturer in the School of Materials Science and Engineering at Changzhou University. He earned his bachelor's degree from Shandong University of Technology in June 2014, and his Ph.D. degree from the Chengdu Institute of Organic Chemistry, Chinese Academy of Sciences, in June 2020. His research focuses on applied basic research in fields related to Si/C anode materials for lithium-ion batteries and carbon-based anode materials for sodium-ion batteries. Over the past three years, he has successfully led five projects, including the National Natural Science Foundation of China Youth Project and the Changzhou Leading Talent Project. Dr. Li has also published 16 papers as the first author/corresponding author and has applied for 8 Chinese invention patents.

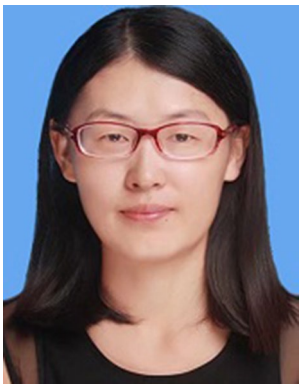

Qian Zhao is now a lecturer in the School of Materials Science and Engineering at Changzhou University. She obtained his Ph.D. degree from Materials Genome Institute of Shanghai University in 2021. Her current research interest focuses on electrochemical energy storage materials and related device systems.

Xiaobing Huang received his B.S degree from Central South University in June 2004 and Ph.D. degree in Chengdu Institute of Organic Chemistry, Chinese Academy of Sciences, in July 2010. He is now a professor in Hunan University of Arts and Science. His research interests focus on new energy storage systems and related electrode materials.

Jianmin Ma is a professor at Tiangong University, Tianjin, China. He serves as the Associate Editor of *Chinese Chemical Letters*, Academic Editor for *Rare Metals*, and is an editorial board member for the *Journal of Energy Chemistry*, *Chinese Chemical Letters*, *Nano-Micro Letters*, *Journal of Physics: Condensed Matter*, *Journal of Physics: Energy*, *Chemistry-An Asian Journal*, and others so on. His research interests focus on electrolytes for energy storage devices.

Yurong Ren is now a professor in the School of Materials Science and Engineering at Changzhou University. She is elected as a Fellow of the Royal Society of Chemistry. She received her bachelor's degree from Jilin Normal University in July 1998 and Ph.D. degree in Chengdu Institute of Organic Chemistry, Chinese Academy of Sciences, in July 2010. She once worked in the University of California, Los Angeles, as a visiting scholar from 2015 to 2016. Her main research topics include new carbon materials and new energy storage materials and related device systems. She has published more than 140 peer-reviewed papers and authorized almost 37 Chinese patents.